BEST AVAILABLE COPY

App Serial # 09/898,456 Exhibit K
Friddle et al. LEX-0198-USA
Novel Human Secreted Proteins and Polynucleotides Encoding the Same

The Sequence of the Human Genome

J. Craig Venter,[1]* Mark D. Adams,[1] Eugene W. Myers,[1] Peter W. Li,[1] Richard J. Mural,[1] Granger G. Sutton,[1] Hamilton O. Smith,[1] Mark Yandell,[1] Cheryl A. Evans,[1] Robert A. Holt,[1] Jeannine D. Gocayne,[1] Peter Amanatides,[1] Richard M. Ballew,[1] Daniel H. Huson,[1] Jennifer Russo Wortman,[1] Qing Zhang,[1] Chinnappa D. Kodira,[1] Xiangqun H. Zheng,[1] Lin Chen,[1] Marian Skupski,[1] Gangadharan Subramanian,[1] Paul D. Thomas,[1] Jinghui Zhang,[1] George L. Gabor Miklos,[2] Catherine Nelson,[3] Samuel Broder,[1] Andrew G. Clark,[4] Joe Nadeau,[5] Victor A. McKusick,[6] Norton Zinder,[7] Arnold J. Levine,[7] Richard J. Roberts,[8] Mel Simon,[9] Carolyn Slayman,[10] Michael Hunkapiller,[11] Randall Bolanos,[1] Arthur Delcher,[1] Ian Dew,[1] Daniel Fasulo,[1] Michael Flanigan,[1] Liliana Florea,[1] Aaron Halpern,[1] Sridhar Hannenhalli,[1] Saul Kravitz,[1] Samuel Levy,[1] Clark Mobarry,[1] Knut Reinert,[1] Karin Remington,[1] Jane Abu-Threideh,[1] Ellen Beasley,[1] Kendra Biddick,[1] Vivien Bonazzi,[1] Rhonda Brandon,[1] Michele Cargill,[1] Ishwar Chandramouliswaran,[1] Rosane Charlab,[1] Kabir Chaturvedi,[1] Zuoming Deng,[1] Valentina Di Francesco,[1] Patrick Dunn,[1] Karen Eilbeck,[1] Carlos Evangelista,[1] Andrei E. Gabrielian,[1] Weiniu Gan,[1] Wangmao Ge,[1] Fangcheng Gong,[1] Zhiping Gu,[1] Ping Guan,[1] Thomas J. Heiman,[1] Maureen E. Higgins,[1] Rui-Ru Ji,[1] Zhaoxi Ke,[1] Karen A. Ketchum,[1] Zhongwu Lai,[1] Yiding Lei,[1] Zhenya Li,[1] Jiayin Li,[1] Yong Liang,[1] Xiaoying Lin,[1] Fu Lu,[1] Gennady V. Merkulov,[1] Natalia Milshina,[1] Helen M. Moore,[1] Ashwinikumar K Naik,[1] Vaibhav A. Narayan,[1] Beena Neelam,[1] Deborah Nusskern,[1] Douglas B. Rusch,[1] Steven Salzberg,[12] Wei Shao,[1] Bixiong Shue,[1] Jingtao Sun,[1] Zhen Yuan Wang,[1] Aihui Wang,[1] Xin Wang,[1] Jian Wang,[1] Ming-Hui Wei,[1] Ron Wides,[13] Chunlin Xiao,[1] Chunhua Yan,[1] Alison Yao,[1] Jane Ye,[1] Ming Zhan,[1] Weiqing Zhang,[1] Hongyu Zhang,[1] Qi Zhao,[1] Liansheng Zheng,[1] Fei Zhong,[1] Wenyan Zhong,[1] Shiaoping C. Zhu,[1] Shaying Zhao,[12] Dennis Gilbert,[1] Suzanna Baumhueter,[1] Gene Spier,[1] Christine Carter,[1] Anibal Cravchik,[1] Trevor Woodage,[1] Feroze Ali,[1] Huijin An,[1] Aderonke Awe,[1] Danita Baldwin,[1] Holly Baden,[1] Mary Barnstead,[1] Ian Barrow,[1] Karen Beeson,[1] Dana Busam,[1] Amy Carver,[1] Angela Center,[1] Ming Lai Cheng,[1] Liz Curry,[1] Steve Danaher,[1] Lionel Davenport,[1] Raymond Desilets,[1] Susanne Dietz,[1] Kristina Dodson,[1] Lisa Doup,[1] Steven Ferriera,[1] Neha Garg,[1] Andres Gluecksmann,[1] Brit Hart,[1] Jason Haynes,[1] Charles Haynes,[1] Cheryl Heiner,[1] Suzanne Hladun,[1] Damon Hostin,[1] Jarrett Houck,[1] Timothy Howland,[1] Chinyere Ibegwam,[1] Jeffery Johnson,[1] Francis Kalush,[1] Lesley Kline,[1] Shashi Koduru,[1] Amy Love,[1] Felecia Mann,[1] David May,[1] Steven McCawley,[1] Tina McIntosh,[1] Ivy McMullen,[1] Mee Moy,[1] Linda Moy,[1] Brian Murphy,[1] Keith Nelson,[1] Cynthia Pfannkoch,[1] Eric Pratts,[1] Vinita Puri,[1] Hina Qureshi,[1] Matthew Reardon,[1] Robert Rodriguez,[1] Yu-Hui Rogers,[1] Deanna Romblad,[1] Bob Ruhfel,[1] Richard Scott,[1] Cynthia Sitter,[1] Michelle Smallwood,[1] Erin Stewart,[1] Renee Strong,[1] Ellen Suh,[1] Reginald Thomas,[1] Ni Ni Tint,[1] Sukyee Tse,[1] Claire Vech,[1] Gary Wang,[1] Jeremy Wetter,[1] Sherita Williams,[1] Monica Williams,[1] Sandra Windsor,[1] Emily Winn-Deen,[1] Keriellen Wolfe,[1] Jayshree Zaveri,[1] Karena Zaveri,[1] Josep F. Abril,[14] Roderic Guigó,[14] Michael J. Campbell,[1] Kimmen V. Sjolander,[1] Brian Karlak,[1] Anish Kejariwal,[1] Huaiyu Mi,[1] Betty Lazareva,[1] Thomas Hatton,[1] Apurva Narechania,[1] Karen Diemer,[1] Anushya Muruganujan,[1] Nan Guo,[1] Shinji Sato,[1] Vineet Bafna,[1] Sorin Istrail,[1] Ross Lippert,[1] Russell Schwartz,[1] Brian Walenz,[1] Shibu Yooseph,[1] David Allen,[1] Anand Basu,[1] James Baxendale,[1] Louis Blick,[1] Marcelo Caminha,[1] John Carnes-Stine,[1] Parris Caulk,[1] Yen-Hui Chiang,[1] My Coyne,[1] Carl Dahlke,[1] Anne Deslattes Mays,[1] Maria Dombroski,[1] Michael Donnelly,[1] Dale Ely,[1] Shiva Esparham,[1] Carl Fosler,[1] Harold Gire,[1] Stephen Glanowski,[1] Kenneth Glasser,[1] Anna Glodek,[1] Mark Gorokhov,[1] Ken Graham,[1] Barry Gropman,[1] Michael Harris,[1] Jeremy Heil,[1] Scott Henderson,[1] Jeffrey Hoover,[1] Donald Jennings,[1] Catherine Jordan,[1] James Jordan,[1] John Kasha,[1] Leonid Kagan,[1] Cheryl Kraft,[1] Alexander Levitsky,[1] Mark Lewis,[1] Xiangjun Liu,[1] John Lopez,[1] Daniel Ma,[1] William Majoros,[1] Joe McDaniel,[1] Sean Murphy,[1] Matthew Newman,[1] Trung Nguyen,[1] Ngoc Nguyen,[1] Marc Nodell,[1] Sue Pan,[1] Jim Peck,[1] Marshall Peterson,[1] William Rowe,[1] Robert Sanders,[1] John Scott,[1] Michael Simpson,[1] Thomas Smith,[1] Arlan Sprague,[1] Timothy Stockwell,[1] Russell Turner,[1] Eli Venter,[1] Mei Wang,[1] Meiyuan Wen,[1] David Wu,[1] Mitchell Wu,[1] Ashley Xia,[1] Ali Zandieh,[1] Xiaohong Zhu[1]

neously map and sequence the human genome by means of end sequences from 150-kbp bacterial artificial chromosomes (BACs) (*17*, *18*). The end sequences spanned by known distances provide long-range continuity across the genome. A modification of the BAC end-sequencing (BES) method was applied successfully to complete chromosome 2 from the *Arabidopsis thaliana* genome (*19*).

In 1997, Weber and Myers (*20*) proposed whole-genome shotgun sequencing of the human genome. Their proposal was not well received (*21*). However, by early 1998, as less than 5% of the genome had been sequenced, it was clear that the rate of progress in human genome sequencing worldwide was very slow (*22*), and the prospects for finishing the genome by the 2005 goal were uncertain.

In early 1998, PE Biosystems (now Applied Biosystems) developed an automated, high-throughput capillary DNA sequencer, subsequently called the ABI PRISM 3700 DNA Analyzer. Discussions between PE Biosystems and TIGR scientists resulted in a plan to undertake the sequencing of the human genome with the 3700 DNA Analyzer and the whole-genome shotgun sequencing techniques developed at TIGR (*23*). Many of the principles of operation of a genome-sequencing facility were established in the TIGR facility (*24*). However, the facility envisioned for Celera would have a capacity roughly 50 times that of TIGR, and thus new developments were required for sample preparation and tracking and for whole-genome assembly. Some argued that the required 150-fold scale-up from the *H. influenzae* genome to the human genome with its complex repeat sequences was not feasible (*25*). The *Drosophila melanogaster* genome was thus chosen as a test case for whole-genome assembly on a large and complex eukaryotic genome. In collaboration with Gerald Rubin and the Berkeley *Drosophila* Genome Project, the nucleotide sequence of the 120-Mbp euchromatic portion of the *Drosophila* genome was determined over a 1-year period (*26*–*28*). The *Drosophila* genome-sequencing effort resulted in two key findings: (i) that the assembly algorithms could generate chromosome assemblies with highly accurate order and orientation with substantially less than 10-fold coverage, and (ii) that undertaking multiple interim assemblies in place of one comprehensive final assembly was not of value.

These findings, together with the dramatic changes in the public genome effort subsequent to the formation of Celera (*29*), led to a modified whole-genome shotgun sequencing approach to the human genome. We initially proposed to do 10-fold sequence coverage of the genome over a 3-year period and to make interim assembled sequence data available quarterly. The modifications included a plan to perform random shotgun sequencing to ~5-fold coverage and to use the unordered and unoriented BAC sequence fragments and subassemblies published in GenBank by the publicly funded genome effort (*30*) to accelerate the project. We also abandoned the quarterly announcements in the absence of interim assemblies to report.

Although this strategy provided a reasonable result very early that was consistent with a whole-genome shotgun assembly with eight-fold coverage, the human genome sequence is not as finished as the *Drosophila* genome was with an effective 13-fold coverage. However, it became clear that even with this reduced coverage strategy, Celera could generate an accurately ordered and oriented scaffold sequence of the human genome in less than 1 year. Human genome sequencing was initiated 8 September 1999 and completed 17 June 2000. The first assembly was completed 25 June 2000, and the assembly reported here was completed 1 October 2000. Here we describe the whole-genome random shotgun sequencing effort applied to the human genome. We developed two different assembly approaches for assembling the ~3 billion bp that make up the 23 pairs of chromosomes of the *Homo sapiens* genome. Any GenBank-derived data were shredded to remove potential bias to the final sequence from chimeric clones, foreign DNA contamination, or misassembled contigs. Insofar as a correctly and accurately assembled genome sequence with faithful order and orientation of contigs is essential for an accurate analysis of the human genetic code, we have devoted a considerable portion of this manuscript to the documentation of the quality of our reconstruction of the genome. We also describe our preliminary analysis of the human genetic code on the basis of computational methods. Figure 1 (see fold-out chart associated with this issue; files for each chromosome can be found in Web fig. 1 on *Science* Online at www.sciencemag.org/cgi/content/full/291/5507/1304/DC1) provides a graphical overview of the genome and the features encoded in it. The detailed manual curation and interpretation of the genome are just beginning.

To aid the reader in locating specific analytical sections, we have divided the paper into seven broad sections. A summary of the major results appears at the beginning of each section.

1 Sources of DNA and Sequencing Methods
2 Genome Assembly Strategy and Characterization
3 Gene Prediction and Annotation
4 Genome Structure
5 Genome Evolution
6 A Genome-Wide Examination of Sequence Variations
7 An Overview of the Predicted Protein-Coding Genes in the Human Genome
8 Conclusions

1 Sources of DNA and Sequencing Methods

Summary. This section discusses the rationale and ethical rules governing donor selection to ensure ethnic and gender diversity along with the methodologies for DNA extraction and library construction. The plasmid library construction is the first critical step in shotgun sequencing. If the DNA libraries are not uniform in size, nonchimeric, and do not randomly represent the genome, then the subsequent steps cannot accurately reconstruct the genome sequence. We used automated high-throughput DNA sequencing and the computational infrastructure to enable efficient tracking of enormous amounts of sequence information (27.3 million sequence reads; 14.9 billion bp of sequence). Sequencing and tracking from both ends of plasmid clones from 2-, 10-, and 50-kbp libraries were essential to the computational reconstruction of the genome. Our evidence indicates that the accurate pairing rate of end sequences was greater than 98%.

Various policies of the United States and the World Medical Association, specifically the Declaration of Helsinki, offer recommendations for conducting experiments with human subjects. We convened an Institutional Review Board (IRB) (*31*) that helped us establish the protocol for obtaining and using human DNA and the informed consent process used to enroll research volunteers for the DNA-sequencing studies reported here. We adopted several steps and procedures to protect the privacy rights and confidentiality of the research subjects (donors). These included a two-stage consent process, a secure random alphanumeric coding system for specimens and records, circumscribed contact with the subjects by researchers, and options for off-site contact of donors. In addition, Celera applied for and received a Certificate of Confidentiality from the Department of Health and Human Services. This Certificate authorized Celera to protect the privacy of the individuals who volunteered to be donors as provided in Section 301(d) of the Public Health Service Act 42 U.S.C. 241(d).

Celera and the IRB believed that the initial version of a completed human genome should be a composite derived from multiple donors of diverse ethnic backgrounds. Prospective donors were asked, on a voluntary basis, to self-designate an ethnogeographic category (e.g., African-American, Chinese, Hispanic, Caucasian, etc.). We enrolled 21 donors (*32*).

Three basic items of information from each donor were recorded and linked by confidential code to the donated sample: age, sex, and self-designated ethnogeographic group. From females, ~130 ml of whole, heparinized blood was collected. From males, ~130 ml of whole, heparinized blood was

nome, and even a modest error rate can reduce the effectiveness of assembly. In addition, maintaining the validity of mate-pair information is absolutely critical for the algorithms described below. Procedural controls were established for maintaining the validity of sequence mate-pairs as sequencing reactions proceeded through the process, including strict rules built into the LIMS. The accuracy of sequence data produced by the Celera process was validated in the course of the *Drosophila* genome project (*26*). By collecting data for the entire human genome in a single facility, we were able to ensure uniform quality standards and the cost advantages associated with automation, an economy of scale, and process consistency.

2 Genome Assembly Strategy and Characterization

Summary. We describe in this section the two approaches that we used to assemble the genome. One method involves the computational combination of all sequence reads with shredded data from GenBank to generate an independent, nonbiased view of the genome. The second approach involves clustering all of the fragments to a region or chromosome on the basis of mapping information. The clustered data were then shredded and subjected to computational assembly. Both approaches provided essentially the same reconstruction of assembled DNA sequence with proper order and orientation. The second method provided slightly greater sequence coverage (fewer gaps) and was the principal sequence used for the analysis phase. In addition, we document the completeness and correctness of this assembly process

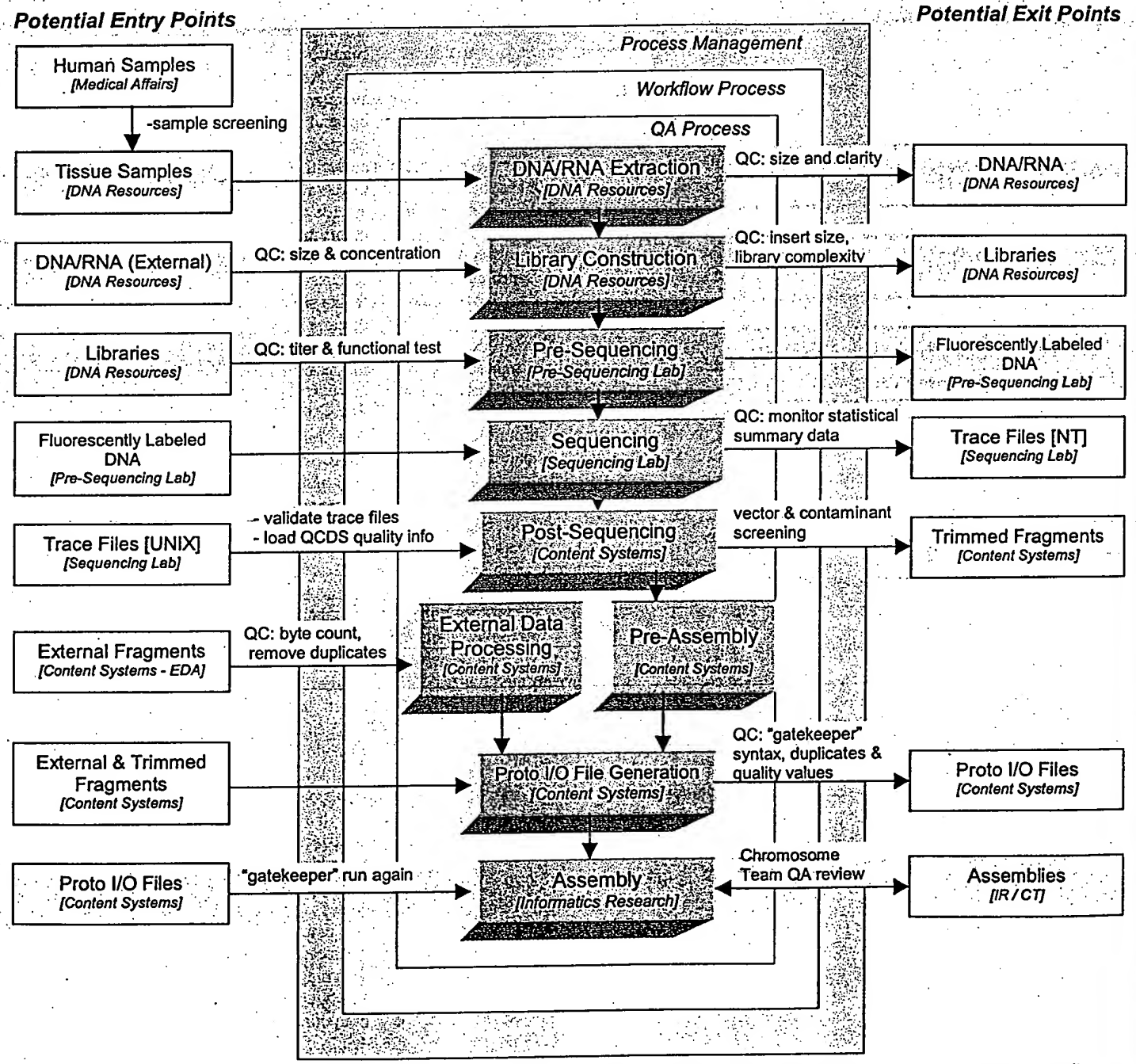

Fig. 2. Flow diagram for sequencing pipeline. Samples are received, selected, and processed in compliance with standard operating procedures, with a focus on quality within and across departments. Each process has defined inputs and outputs with the capability to exchange samples and data with both internal and external entities according to defined quality guidelines. Manufacturing pipeline processes, products, quality control measures, and responsible parties are indicated and are described further in the text.

information was ignored because some BACs were not correctly placed on the PFP physical map and because we found strong evidence that at least 2.2% of the BACs contained sequence data that were not part of the given BAC (*41*), possibly as a result of sample-tracking errors (see below). In short, we performed a true, ab initio whole-genome assembly in which we took the expedient of deriving additional sequence coverage, but not mate pairs, assembled bactigs, or genome locality, from some externally generated data.

In the compartmentalized shotgun assembly (CSA), Celera and PFP data were partitioned into the largest possible chromosomal segments or "components" that could be determined with confidence, and then shotgun assembly was applied to each partitioned subset wherein the bactig data were again shredded into faux reads to ensure an independent ab initio assembly of the component. By subsetting the data in this way, the overall computational effort was reduced and the effect of interchromosomal duplications was ameliorated. This also resulted in a reconstruction of the genome that was relatively independent of the whole-genome assembly results so that the two assemblies could be compared for consistency. The quality of the partitioning into components was crucial so that different genome regions were not mixed together. We constructed components from (i) the longest scaffolds of the sequence from each BAC and (ii) assembled scaffolds of data unique to Celera's data set. The BAC assemblies were obtained by a combining assembler that used the bactigs and the 5× Celera data mapped to those bactigs as input. This effort was undertaken as an interim step solely because the more accurate and complete the scaffold for a given sequence stretch, the more accurately one can tile these scaffolds into contiguous components on the basis of sequence overlap and mate-pair information. We further visually inspected and curated the scaffold tiling of the components to further increase its accuracy. For the final CSA assembly, all but the partitioning was ignored, and an independent, ab initio reconstruction of the sequence in each component was obtained by applying our whole-genome assembly algorithm to the partitioned, relevant Celera data and the shredded, faux reads of the partitioned, relevant bactig data.

Table 2. GenBank data input into assembly.

Center	Statistics	Completion phase sequence		
		0	1 and 2	3
Whitehead Institute/ MIT Center for Genome Research, USA	Number of accession records	2,825	6,533	363
	Number of contigs	243,786	138,023	363
	Total base pairs	194,490,158	1,083,848,245	48,829,358
	Total vector masked (bp)	1,553,597	875,618	2,202
	Total contaminant masked (bp)	13,654,482	4,417,055	98,028
	Average contig length (bp)	798	7,853	134,516
Washington University, USA	Number of accession records	19	3,232	1,300
	Number of contigs	2,127	61,812	1,300
	Total base pairs	1,195,732	561,171,788	164,214,395
	Total vector masked (bp)	21,604	270,942	8,287
	Total contaminant masked (bp)	22,469	1,476,141	469,487
	Average contig length (bp)	562	9,079	126,319
Baylor College of Medicine, USA	Number of accession records	0	1,626	363
	Number of contigs	0	44,861	363
	Total base pairs	0	265,547,066	49,017,104
	Total vector masked (bp)	0	218,769	4,960
	Total contaminant masked (bp)	0	1,784,700	485,137
	Average contig length (bp)	0	5,919	135,033
Production Sequencing Facility, DOE Joint Genome Institute, USA	Number of accession records	135	2,043	754
	Number of contigs	7,052	34,938	754
	Total base pairs	8,680,214	294,249,631	60,975,328
	Total vector masked (bp)	22,644	162,651	7,274
	Total contaminant masked (bp)	665,818	4,642,372	118,387
	Average contig length (bp)	1,231	8,422	80,867
The Institute of Physical and Chemical Research (RIKEN), Japan	Number of accession records	0	1,149	300
	Number of contigs	0	25,772	300
	Total base pairs	0	182,812,275	20,093,926
	Total vector masked (bp)	0	203,792	2,371
	Total contaminant masked (bp)	0	308,426	27,781
	Average contig length (bp)	0	7,093	66,978
Sanger Centre, UK	Number of accession records	0	4,538	2,599
	Number of contigs	0	74,324	2,599
	Total base pairs	0	689,059,692	246,118,000
	Total vector masked (bp)	0	427,326	25,054
	Total contaminant masked (bp)	0	2,066,305	374,561
	Average contig length (bp)	0	9,271	94,697
Others*	Number of accession records	42	1,894	3,458
	Number of contigs	5,978	29,898	3,458
	Total base pairs	5,564,879	283,358,877	246,474,157
	Total vector masked (bp)	57,448	279,477	32,136
	Total contaminant masked (bp)	575,366	1,616,665	1,791,849
	Average contig length (bp)	931	9,478	71,277
All centers combined†	Number of accession records	3,021	21,015	9,137
	Number of contigs	258,943	409,628	9,137
	Total base pairs	209,930,983	3,360,047,574	835,722,268
	Total vector masked (bp)	1,655,293	2,438,575	82,284
	Total contaminant masked (bp)	14,918,135	16,311,664	3,365,230
	Average contig length (bp)	811	8,203	91,466

*Other centers contributing at least 0.1% of the sequence include: Chinese National Human Genome Center; Genomanalyse Gesellschaft fuer Biotechnologische Forschung mbH; Genome Therapeutics Corporation; GENOSCOPE; Chinese Academy of Sciences; Institute of Molecular Biotechnology; Keio University School of Medicine; Lawrence Livermore National Laboratory; Cold Spring Harbor Laboratory; Los Alamos National Laboratory; Max-Planck Institut fuer Molekulare, Genetik; Japan Science and Technology Corporation; Stanford University; The Institute for Genomic Research; The Institute of Physical and Chemical Research, Gene Bank; The University of Oklahoma; University of Texas Southwestern Medical Center, University of Washington. †The 4,405,700,825 bases contributed by all centers were shredded into faux reads resulting in 2.96× coverage of the genome.

2.3 Whole-genome assembly

The algorithms used for whole-genome assembly (WGA) of the human genome were enhancements to those used to produce the sequence of the *Drosophila* genome reported in detail in (*28*).

The WGA assembler consists of a pipeline composed of five principal stages: Screener, Overlapper, Unitigger, Scaffolder, and Repeat Resolver, respectively. The Screener finds and marks all microsatellite repeats with less than a 6-bp element, and screens out all known interspersed repeat elements, including Alu, Line, and ribosomal DNA. Marked regions get searched for overlaps, whereas screened regions do not get searched, but can be part of an overlap that involves unscreened matching segments.

some 22, all stones were placed correctly.

The final method of resolving gaps is to fill them with assembled BAC data that cover the gap. We call this external gap "walking." We did not include the very aggressive "Pebbles" substage described in our *Drosophila* work, which made enough mistakes so as to produce repeat reconstructions for long interspersed elements whose quality was only 99.62% correct. We decided that for the human genome it was philosophically better not to introduce a step that was certain to produce less than 99.99% accuracy. The cost was a somewhat larger number of gaps of somewhat larger size.

At the final stage of the assembly process, and also at several intermediate points, a consensus sequence of every contig is produced. Our algorithm is driven by the principle of maximum parsimony, with quality-value–weighted measures for evaluating each base. The net effect is a Bayesian estimate of the correct base to report at each position. Consensus generation uses Celera data whenever it is present. In the event that no Celera data cover a given region, the BAC data sequence is used.

A key element of achieving a WGA of the human genome was to parallelize the Overlapper and the central consensus sequence–constructing subroutines. In addition, memory was a real issue—a straightforward application of the software we had built for *Drosophila* would have required a computer with a 600-gigabyte RAM. By making the Overlapper and Unitigger incremental, we were able to achieve the same computation with a maximum of instantaneous usage of 28 gigabytes of RAM. Moreover, the incremental nature of the first three stages allowed us to continually update the state of this part of the computation as data were delivered and then perform a 7-day run to complete Scaffolding and Repeat Resolution whenever desired. For our assembly operations, the total compute infrastructure consists of 10 four-processor SMPs with 4 gigabytes of memory per cluster (Compaq's ES40, Regatta) and a 16-processor NUMA machine with 64 gigabytes of memory (Compaq's GS160, Wildfire). The total compute for a run of the assembler was roughly 20,000 CPU hours.

The assembly of Celera's data, together with the shredded bactig data, produced a set of scaffolds totaling 2.848 Gbp in span and consisting of 2.586 Gbp of sequence. The chaff, or set of reads not incorporated in the assembly, numbered 11.27 million (26%), which is consistent with our experience for *Drosophila*. More than 84% of the genome was covered by scaffolds >100 kbp long, and these averaged 91% sequence and 9% gaps with a total of 2.297 Gbp of sequence. There were a total of 93,857 gaps among the 1637 scaffolds >100 kbp. The average scaffold size was 1.5 Mbp, the average contig size was 24.06 kbp, and the average gap size was 2.43 kbp, where the distribution of each was essentially exponential. More than 50% of all gaps were less than 500 bp long, >62% of all gaps were less than 1 kbp long, and no gap was >100 kbp long. Similarly, more than 65% of the sequence is in contigs >30 kbp, more than 31% is in contigs >100 kbp, and the largest contig was 1.22 Mbp long. Table 3 gives detailed summary statistics for the structure of this assembly with a direct comparison to the compartmentalized shotgun assembly.

2.4 Compartmentalized shotgun assembly

In addition to the WGA approach, we pursued a localized assembly approach that was intended to subdivide the genome into segments, each of which could be shotgun assembled individually. We expected that this would help in resolution of large interchromosomal duplications and improve the statistics for calculating U-unitigs. The compartmentalized assembly process involved clustering Celera reads and bactigs into large, multiple megabase regions of the genome, and then running the WGA assembler on the Celera data and shredded, faux reads obtained from the bactig data.

The first phase of the CSA strategy was to separate Celera reads into those that matched the BAC contigs for a particular PFP BAC entry, and those that did not match any public data. Such matches must be guaranteed to

Table 3. Scaffold statistics for whole-genome and compartmentalized shotgun assemblies.

	Scaffold size				
	All	>30 kbp	>100 kbp	>500 kbp	>1000 kbp
	Compartmentalized shotgun assembly				
No. of bp in scaffolds (including intrascaffold gaps)	2,905,568,203	2,748,892,430	2,700,489,906	2,489,357,260	2,248,689,128
No. of bp in contigs	2,653,979,733	2,524,251,302	2,491,538,372	2,320,648,201	2,106,521,902
No. of scaffolds	53,591	2,845	1,935	1,060	721
No. of contigs	170,033	112,207	107,199	93,138	82,009
No. of gaps	116,442	109,362	105,264	92,078	81,288
No. of gaps ≤1 kbp	72,091	69,175	67,289	59,915	53,354
Average scaffold size (bp)	54,217	966,219	1,395,602	2,348,450	3,118,848
Average contig size (bp)	15,609	22,496	23,242	24,916	25,686
Average intrascaffold gap size (bp)	2,161	2,054	1,985	1,832	1,749
Largest contig (bp)	1,988,321	1,988,321	1,988,321	1,988,321	1,988,321
% of total contigs	100	95	94	87	79
	Whole-genome assembly				
No. of bp in scaffolds (including intrascaffold gaps)	2,847,890,390	2,574,792,618	2,525,334,447	2,328,535,466	2,140,943,032
No. of bp in contigs	2,586,634,108	2,334,343,339	2,297,678,935	2,143,002,184	1,983,305,432
No. of scaffolds	118,968	2,507	1,637	818	554
No. of contigs	221,036	99,189	95,494	84,641	76,285
No. of gaps	102,068	96,682	93,857	83,823	75,731
No. of gaps ≤1 kbp	62,356	60,343	59,156	54,079	49,592
Average scaffold size (bp)	23,938	1,027,041	1,542,660	2,846,620	3,864,518
Average contig size (bp)	11,702	23,534	24,061	25,319	25,999
Average intrascaffold gap size (bp)	2,560	2,487	2,426	2,213	2,082
Largest contig (bp)	1,224,073	1,224,073	1,224,073	1,224,073	1,224,073
% of total contigs	100	90	89	83	77

not covered by a matching segment in the other assembly. Some 82.5 Mbp of the WGA (3.95%) was not covered by the CSA, whereas 204.5 Mbp (8.26%) of the CSA was not covered by the WGA. This estimate did not require any consistency of the assemblies or any uniqueness of the matching segments. Thus, another analysis was conducted in which matches of less than 1 kbp between a pair of scaffolds were excluded unless they were confirmed by other matches having a consistent order and orientation. This gives some measure of consistent coverage: 1.982 Gbp (95.00%) of the WGA is covered by the CSA, and 2.169 Gbp (87.69%) of the CSA is covered by the WGA by this more stringent measure.

The comparison of WGA to CSA also permitted evaluation of scaffolds for structural inconsistencies. We looked for instances in which a large section of a scaffold from one assembly matched only one scaffold from the other assembly, but failed to match over the full length of the overlap implied by the matching segments. An initial set of candidates was identified automatically, and then each candidate was inspected by hand. From this process, we identified 31 instances in which the assemblies appear to disagree in a nonlocal fashion. These cases are being further evaluated to determine which assembly is in error and why.

In addition, we evaluated local inconsistencies of order or orientation. The following results exclude cases in which one contig in one assembly corresponds to more than one overlapping contig in the other assembly (as long as the order and orientation of the latter agrees with the positions they match in the former). Most of these small rearrangements involved segments on the order of hundreds of base pairs and rarely >1 kbp. We found a total of 295 kbp (0.012%) in the CSA assemblies that were locally inconsistent with the WGA assemblies, whereas 2.108 Mbp (0.11%) in the WGA assembly were inconsistent with the CSA assembly.

The CSA assembly was a few percentage points better in terms of coverage and slightly more consistent than the WGA, because it was in effect performing a few thousand shotgun assemblies of megabase-sized problems, whereas the WGA is performing a shotgun assembly of a gigabase-sized problem. When one considers the increase of two-and-a-half orders of magnitude in problem size, the information loss between the two is remarkably small. Because CSA was logistically easier to deliver and the better of the two results available at the time when downstream analyses needed to be begun, all subsequent analysis was performed on this assembly.

2.6 Mapping scaffolds to the genome

The final step in assembling the genome was to order and orient the scaffolds on the chromosomes. We first grouped scaffolds together on the basis of their order in the components from CSA. These grouped scaffolds were reordered by examining residual mate-pairing data between the scaffolds. We next mapped the scaffold groups onto the chromosome using physical mapping data. This step depends on having reliable high-resolution map information such that each scaffold will overlap multiple markers. There are two genome-wide types of map information available: high-density STS maps and fingerprint maps of BAC clones developed at Washington University (*45*). Among the genome-wide STS maps, GeneMap99 (GM99) has the most markers and therefore was most useful for mapping scaffolds. The two different mapping approaches are complementary to one another. The fingerprint maps should have better local order because they were built by comparison of overlapping BAC clones. On the other hand, GM99 should have a more reliable long-range order, because the framework markers were derived from well-validated genetic maps. Both types of maps were used as a reference for human curation of the components that were the input to the regional assembly, but they did not determine the order of sequences produced by the assembler.

In order to determine the effectiveness of the fingerprint maps and GM99 for mapping scaffolds, we first examined the reliability of these maps by comparison with large scaffolds. Only 1% of the STS markers on the 10 largest scaffolds (those >9 Mbp) were mapped on a different chromosome on GM99. Two percent of the STS markers disagreed in position by more than five framework bins. However, for the fingerprint maps, a 2% chromosome discrepancy was observed, and on average 23.8% of BAC locations in the scaffold sequence disagreed with fingerprint map placement by more than five BACs. When further examining the source of discrepancy, it was found that most of the discrepancy came from 4 of the 10 scaffolds, indicating this there is variation in the quality of either the map or the scaffolds. All four scaffolds were assembled, as well as the other six, as judged by clone coverage analysis, and showed the same low discrepancy rate to GM99, and thus we concluded that the fingerprint map global order in these cases was not reliable. Smaller scaffolds had a higher discordance rate with GM99 (4.21% of STSs were discordant by more than five framework bins), but a lower discordance rate with the fingerprint maps (11% of BACs disagreed with fingerprint maps by more than five BACs). This observation agrees with the clone coverage analysis (*46*) that Celera scaffold construction was better supported by long-range mate pairs in larger scaffolds than in small scaffolds.

We created two orderings of Celera scaffolds on the basis of the markers (BAC or STS) on these maps. Where the order of scaffolds agreed between GM99 and the WashU BAC map, we had a high degree of confidence that that order was correct; these scaffolds were termed "anchor scaffolds." Only scaffolds with a low overall discrepancy rate with both maps were considered anchor scaffolds. Scaffolds in GM99 bins were allowed to permute in their order to match WashU ordering, provided they did not violate their framework orders. Orientation of individual scaffolds was determined by the presence of multiple mapped markers with consistent order. Scaffolds with only one marker have insufficient information to assign orientation. We found 70.1% of the genome in anchored scaffolds, more than 99% of which are also oriented (Table 4). Because GM99 is of lower resolution than the WashU map, a number of scaffolds without STS matches could be ordered relative to the anchored scaffolds because they included sequence from the same or adjacent BACs on the WashU map. On the other hand, because of occasional WashU global ordering discrepancies, a number of scaffolds determined to be "unmappable" on the WashU map could be ordered relative to the anchored scaffolds

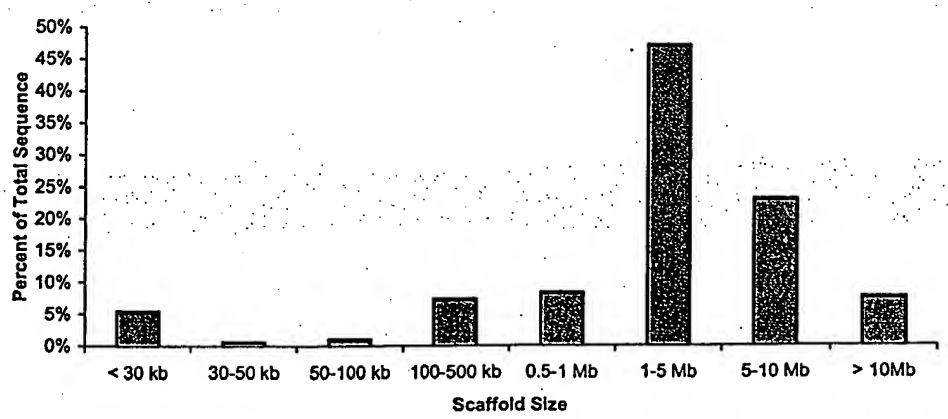

Fig. 5. Distribution of scaffold sizes of the CSA. For each range of scaffold sizes, the percent of total sequence is indicated.

sembly against other finished sequence for determining sequencing accuracy at the nucleotide level, although this has been done for identifying polymorphisms as described in Section 6. The accuracy of the consensus sequence is at least 99.96% on the basis of a statistical estimate derived from the quality values of the underlying reads.

The structural consistency of the assembly can be measured by mate-pair analysis. In a correct assembly, every mated pair of sequencing reads should be located on the consensus sequence with the correct separation and orientation between the pairs. A pair is termed "valid" when the reads are in the correct orientation and the distance between them is within the mean ± 3 standard deviations of the distribution of insert sizes of the library from which the pair was sampled. A pair is termed "misoriented" when the reads are not correctly oriented, and is termed "misseparated" when the distance between the reads is not in the correct range but the reads are correctly oriented. The mean ± the standard deviation of each library used by the assembler was determined as described above. To validate these, we examined all reads mapped to the finished sequence of chromosome 21 (*48*) and determined how many incorrect mate pairs there were as a result of laboratory tracking errors and chimerism (two different segments of the genome cloned into the same plasmid), and how tight the distribution of insert sizes was for those that were correct (Table 5). The standard deviations for all Celera libraries were quite small, less than 15% of the insert length, with the exception of a few 50-kbp libraries. The 2- and 10-kbp libraries contained less than 2% invalid mate pairs, whereas the 50-kbp libraries were somewhat higher (~10%). Thus, although the mate-pair information was not perfect, its accuracy was such that measuring valid, misoriented, and misseparated pairs with respect to a given assembly was deemed to be a reliable instrument for validation purposes, especially when several mate pairs confirm or deny an ordering.

The clone coverage of the genome was 39×, meaning that any given base pair was, on average, contained in 39 clones or, equivalently, spanned by 39 mate-paired reads. Areas of low clone coverage or areas with a high proportion of invalid mate pairs would indicate potential assembly problems. We computed the coverage of each base in the assembly by valid mate pairs (Table 6). In summary, for scaffolds >30 kbp in length, less than 1% of the Celera assembly was in regions of less than 3× clone coverage. Thus, more than 99% of the assembly, including order and orientation, is strongly supported by this measure alone.

We examined the locations and number of all misoriented and misseparated mates. In addition to doing this analysis on the CSA assembly (as of 1 October 2000), we also performed a study of the PFP assembly as of 5 September 2000 (*30*, *55b*). In this latter case, Celera mate pairs had to be mapped to the PFP assembly. To avoid mapping errors due to high-fidelity repeats, the only pairs mapped were those for which both reads matched at only one location with less than 6% differences. A threshold was set such that sets of five or more simultaneously invalid mate pairs indicated a potential breakpoint, where the construction of the two assemblies differed. The graphic comparison of the CSA chromosome 21 assembly with the published sequence (Fig. 6A) serves as a validation of this methodology. Blue tick marks in the panels indicate breakpoints. There were a similar (small) number of breakpoints on both chromosome sequences. The exception was 12 sets of scaffolds in the Celera assembly (a total of 3% of the chromosome length in 212 single-contig scaffolds) that were mapped to the wrong positions because they were too small to be mapped reliably. Figures 6 and 7 and Table 6 illustrate the mate-pair differences and breakpoints between the two assemblies. There was a higher percentage of misoriented and misseparated mate pairs in the large-insert libraries (50 kbp and BAC ends) than in the small-insert libraries in both assemblies (Table 6). The large-insert libraries are more likely to identify discrepancies simply because they span a larger segment of the genome. The graphic comparison between the two assemblies for chromosome 8 (Fig. 6, B and C) shows that there are many

Table 5. Mate-pair validation. Celera fragment sequences were mapped to the published sequence of chromosome 21. Each mate pair uniquely mapped was evaluated for correct orientation and placement (number of mate pairs tested). If the two mates had incorrect relative orientation or placement, they were considered invalid (number of invalid mate pairs).

		Chromosome 21						Genome		
Library type	Library no.	Mean insert size (bp)	SD (bp)	SD/ mean (%)	No. of mate pairs tested	No. of invalid mate pairs	% invalid	Mean insert size (bp)	SD (bp)	SD/ mean (%)
2 kbp	1	2,081	106	5.1	3,642	38	1.0	2,082	90	4.3
	2	1,913	152	7.9	28,029	413	1.5	1,923	118	6.1
	3	2,166	175	8.1	4,405	57	1.3	2,162	158	7.3
10 kbp	4	11,385	851	7.5	4,319	80	1.9	11,370	696	6.1
	5	14,523	1,875	12.9	7,355	156	2.1	14,142	1,402	9.9
	6	9,635	1,035	10.7	5,573	109	2.0	9,606	934	9.7
	7	10,223	928	9.1	34,079	399	1.2	10,190	777	7.6
50 kbp	8	64,888	2,747	4.2	16	1	6.3	65,500	5,504	8.4
	9	53,410	5,834	10.9	914	170	18.6	53,311	5,546	10.4
	10	52,034	7,312	14.1	5,871	569	9.7	51,498	6,588	12.8
	11	52,282	7,454	14.3	2,629	213	8.1	52,282	7,454	14.3
	12	46,616	7,378	15.8	2,153	215	10.0	45,418	9,068	20.0
	13	55,788	10,099	18.1	2,244	249	11.1	53,062	10,893	20.5
	14	39,894	5,019	12.6	199	7	3.5	36,838	9,988	27.1
BES	15	48,931	9,813	20.1	144	10	6.9	47,845	4,774	10.0
	16	48,130	4,232	8.8	195	14	7.2	47,924	4,581	9.6
	17	106,027	27,778	26.2	330	16	4.8	152,000	26,600	17.5
	18	160,575	54,973	34.2	155	8	5.2	161,750	27,000	16.7
	19	164,155	19,453	11.9	642	44	6.9	176,500	19,500	11.05
Sum					102,894	2,768 (mean = 2.7)	2.7			

gene boundaries. During this process, multiple hits to the same region were collapsed to a coherent set of data by tracking the coverage of a region. For example, if a group of bases was represented by multiple overlapping ESTs, the union of these regions matched by the set of ESTs on the scaffold was marked as being supported by EST evidence. This resulted in a series of "gene bins," each of which was believed to contain a single gene. One weakness of this initial implementation of the algorithm was in predicting gene boundaries in regions of tandemly duplicated genes. Gene clusters frequently resulted in homologous neighboring genes being joined together, resulting in an annotation that artificially concatenated these gene models.

Next, known genes (those with exact matches of a full-length cDNA sequence to the genome) were identified, and the region corresponding to the cDNA was annotated as a predicted transcript. A subset of the curated human gene set RefSeq from the National Center for Biotechnology Information (NCBI) was included as a data set searched in the computational pipeline. If a RefSeq transcript matched the genome assembly for at least 50% of its length at >92% identity, then the SIM4 (*63*) alignment of the RefSeq transcript to the region of the genome under analysis was promoted to the status of an Otto annotation. Because the genome sequence has gaps and sequence errors such as frameshifts, it was not always possible to predict a transcript that agrees precisely with the experimentally determined cDNA sequence. A total of 6538 genes in our inventory were identified and transcripts predicted in this way.

Regions that have a substantial amount of sequence similarity, but do not match known genes, were analyzed by that part of the Otto system that uses the sequence similarity information to predict a transcript. Here, Otto

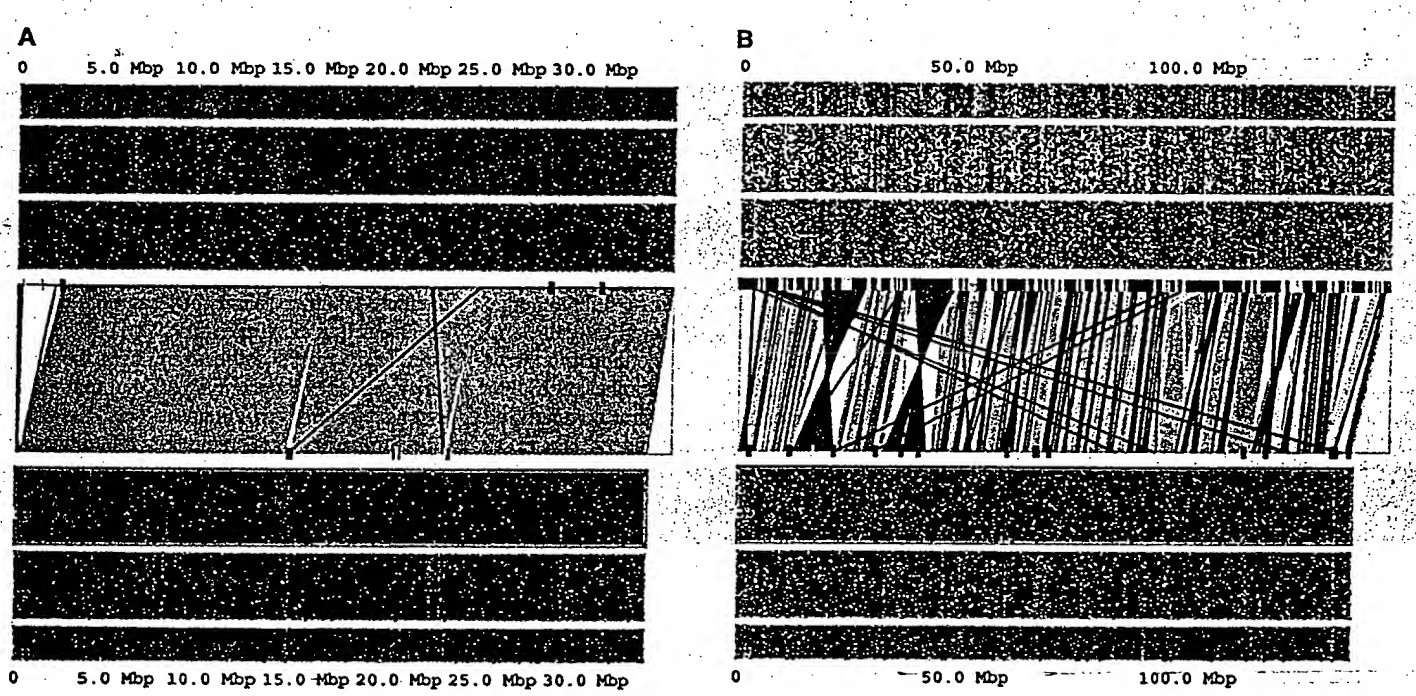

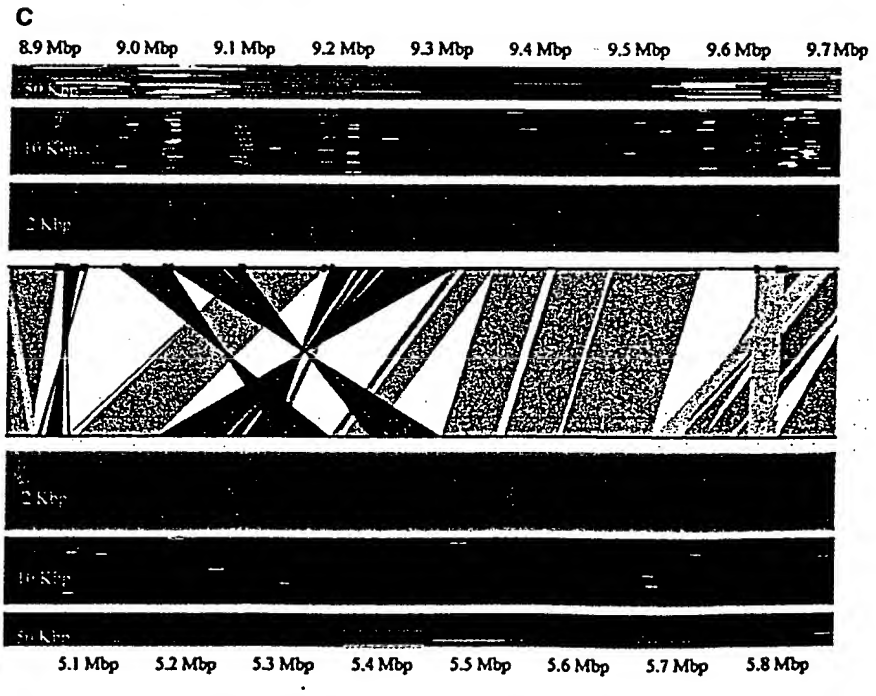

Fig. 6. Comparison of the CSA and the PFP assembly. (A) All of chromosome 21, (B) all of chromosome 8, and (C) a 1-Mb region of chromosome 8 representing a single Celera scaffold. To generate the figure, Celera fragment sequences were mapped onto each assembly. The PFP assembly is indicated in the upper third of each panel; the Celera assembly is indicated in the lower third. In the center of the panel, green lines show Celera sequences that are in the same order and orientation in both assemblies and form the longest consistently ordered run of sequences. Yellow lines indicate sequence blocks that are in the same orientation, but out of order. Red lines indicate sequence blocks that are not in the same orientation. For clarity, in the latter two cases, lines are only drawn between segments of matching sequence that are at least 50 kbp long. The top and bottom thirds of each panel show the extent of Celera mate-pair violations (red, misoriented; yellow, incorrect distance between the mates) for each assembly grouped by library size. (Mate pairs that are within the correct distance, as expected from the mean library insert size, are omitted from the figure for clarity.) Predicted breakpoints, corresponding to stacks of violated mate pairs of the same type, are shown as blue ticks on each assembly axis. Runs of more than 10,000 Ns are shown as cyan bars. Plots of all 24 chromosomes can be seen in Web fig. 3 on *Science* Online at www.sciencemag.org/cgi/content/full/291/5507/1304/DC1.

bases flanking these regions). The other bases in the region, those not covered by any homology evidence, were replaced by N's. This sequence segment, with high confidence regions represented by the consensus genomic sequence and the remainder represented by N's, was then evaluated by Genscan to see if a consistent gene model could be generated. This procedure simplified the gene-prediction task by first establishing the boundary for the gene (not a strength of most gene-finding algorithms), and by eliminating regions with no supporting evidence. If Genscan returned a plausible gene model, it was further evaluated before being promoted to an "Otto" annotation. The final Genscan predictions were often quite different from the prediction that Genscan returned on the same region of native genomic sequence. A weakness of using Genscan to refine the gene model is the loss of valid, small exons from the final annotation.

The next step in defining gene structures based on sequence similarity was to compare each predicted transcript with the homology-based evidence that was used in previous steps to evaluate the depth of evidence for each exon in the prediction. Internal exons were considered to be supported if they were covered by homology evidence to within ±10 bases of their edges. For first and last exons, the internal edge was required to be within 10 bases, but the external edge was allowed greater latitude to allow for 5′ and 3′ untranslated regions (UTRs). To be retained, a prediction for a multi-exon gene must have evidence such that the total number of "hits," as defined above, divided by the number of exons in the prediction must be >0.66 or must correspond to a RefSeq sequence. A single-exon gene must be covered by at least three supporting hits (±10 bases on each side), and these must cover the complete predicted open reading frame. For a single-exon gene, we also required that the Genscan prediction include both a start and a stop codon. Gene models that did not meet these criteria were disregarded, and those that passed were promoted to Otto predictions. Homology-based Otto predictions do not contain 3′ and 5′ untranslated sequence. Although three de novo gene-finding programs [GRAIL, Genscan, and FgenesH (*63*)] were run as part of the computational analysis, the results of these programs were not directly used in making the Otto predictions. Otto predicted 11,226 additional genes by means of sequence similarity.

Table 7. Sensitivity and specificity of Otto and Genscan. Sensitivity and specificity were calculated by first aligning the prediction to the published RefSeq transcript, tallying the number (*N*) of uniquely aligned RefSeq bases. Sensitivity is the ratio of *N* to the length of the published RefSeq transcript. Specificity is the ratio of *N* to the length of the prediction. All differences are significant (Tukey HSD; $P < 0.001$).

Method	Sensitivity	Specificity
Otto (RefSeq only)*	0.939	0.973
Otto (homology)†	0.604	0.884
Genscan	0.501	0.633

*Refers to those annotations produced by Otto using only the Sim4-polished RefSeq alignment rather than an evidence-based Genscan prediction. †Refers to those annotations produced by supplying all available evidence to Genscan.

3.2 Otto validation

To validate the Otto homology-based process and the method that Otto uses to define the structures of known genes, we compared transcripts predicted by Otto with their corresponding (and presumably correct) transcript from a set of 4512 RefSeq transcripts for which there was a unique SIM4 alignment (Table 7). In order to evaluate the relative performance of Otto and Genscan, we made three comparisons. The first involved a determination of the accuracy of gene models predicted by Otto with only homology data other than the corresponding RefSeq sequence (Otto homology in Table 7). We measured the sensitivity (correctly predicted bases divided by the total length of the cDNA) and specificity (correctly predicted bases divided by the sum of the correctly and incorrectly predicted bases). Second, we examined the sensitivity and specificity of the Otto predictions that were made solely with the RefSeq sequence, which is the process that Otto uses to annotate known genes (Otto-RefSeq). And third, we determined the accuracy of the Genscan predictions corresponding to these RefSeq sequences. As expected, the alignment method (Otto-RefSeq) was the most accurate, and Otto-homology performed better than Genscan by both criteria. Thus, 6.1% of true RefSeq nucleotides were not represented in the Otto-refseq annotations and 2.7% of the nucleotides in the Otto-RefSeq transcripts were not contained in the original RefSeq transcripts. The discrepancies could come from legitimate differences between the Celera assembly and the RefSeq transcript due to polymorphisms, incomplete or incorrect data in the Celera assembly, errors introduced by Sim4 during the alignment process, or the presence of alternatively spliced forms in the data set used for the comparisons.

Because Otto uses an evidence-based approach to reconstruct genes, the absence of experimental evidence for intervening exons may inadvertantly result in a set of exons that cannot be spliced together to give rise to a transcript. In such cases, Otto may "split genes" when in fact all the evidence should be combined into a single transcript. We also examined the tendency of these methods to incorrectly split gene predictions. These trends are shown in Fig. 8. Both RefSeq and homology-based predictions by Otto split known genes into fewer segments than Genscan alone.

3.3 Gene number

Recognizing that the Otto system is quite conservative, we used a different gene-prediction strategy in regions where the homology evidence was less strong. Here the results of de novo gene predictions were used. For these genes, we insisted that a predicted transcript have at least two of the following types of evidence to be included in the gene set for further analysis: protein, human EST, rodent EST, or mouse genome fragment matches. This final class of predicted genes is a subset of the predictions made by the three gene-finding programs that were used in the computational pipeline. For these, there was not sufficient sequence similarity information for Otto to attempt to predict a gene structure. The three de novo gene-finding programs resulted in about 155,695 predictions, of which ~76,410 were nonredundant (nonoverlapping with one another). Of these, 57,935 did not overlap known genes or predictions made by Otto. Only 21,350 of the gene predictions that did not overlap Otto predictions were partially supported by at least one type of sequence similarity evidence, and 8619 were partially supported by two types of evidence (Table 8).

The sum of this number (21,350) and the number of Otto annotations (17,764), 39,114, is near the upper limit for the human gene complement. As seen in Table 8, if the requirement for other supporting evidence is made more stringent, this number drops rapidly so that demanding two types of evidence reduces the total gene number to 26,383 and demanding three types reduces it to ~23,000. Requiring that a prediction be supported by all four categories of evidence is too stringent because it would eliminate genes that encode novel proteins (members of currently undescribed protein families). No correction for pseudogenes has been made at this point in the analysis.

In a further attempt to identify genes that were not found by the autoannotation process or any of the de novo gene finders, we examined regions outside of gene predictions that were similar to the EST sequence, and where the EST matched the genomic sequence across a splice junction. After correcting for potential 3′ UTRs of predicted genes, about 2500 such regions remained. Addition of a requirement for at least one of the following evidence types—homology to mouse genomic sequence fragments, rodent ESTs, or cDNAs—or similarity to a known protein reduced this number to 1010. Adding this to the numbers from the previous paragraph would give us estimates of about 40,000, 27,000, and 24,000 potential genes in the human genome, depending on the stringency of evidence considered. Table 8 illustrates the number of genes and presents the degree of

Examination of pericentromeric regions is ongoing.

The remaining ~80% of the genome, the euchromatic component, is divisible into G-, R-, and T-bands (*67*). These cytogenetic bands have been presumed to differ in their nucleotide composition and gene density, although we have been unable to determine precise band boundaries at the molecular level. T-bands are the most G+C- and gene-rich, and G-bands are G+C-poor (*68*). Bernardi has also offered a description of the euchromatin at the molecular level as long stretches of DNA of differing base composition, termed isochores (denoted L, H1, H2, and H3), which are >300 kbp in length (*69*). Bernardi defined the L (light) isochores as G+C-poor (<43%), whereas the H (heavy) isochores fall into three G+C-rich classes representing 24, 8, and 5% of the genome. Gene concentration has been claimed to be very low in the L isochores and 20-fold more enriched in the H2 and H3 isochores (*70*). By examining contiguous 50-kbp windows of G+C content across the assembly, we found that regions of G+C content >48% (H3 isochores) averaged 273.9 kbp in length, those with G+C content between 43 and 48% (H1+H2 isochores) averaged 202.8 kbp in length, and the average span of regions with <43% (L isochores) was 1078.6 kbp. The correlation between G+C content and gene density was also examined in 50-kbp windows along the assembled sequence (Table 9 and Figs. 10 and 11). We found that the density of genes was greater in regions of high G+C than in regions of low G+C content, as expected. However, the correlation between G+C content and gene density was not as skewed as previously predicted (*69*). A higher proportion of genes were located in the G+C-poor regions than had been expected.

Chromosomes 17, 19, and 22, which have a disproportionate number of H3-containing bands, had the highest gene density (Table 10). Conversely, of the chromosomes that we found to have the lowest gene density, X, 4, 18, 13, and Y, also have the fewest H3 bands. Chromosome 15, which also has few H3 bands, did not have a particularly low gene density in our analysis. In addition, chromosome 8, which we found to have a low gene density, does not appear to be unusual in its H3 banding.

How valid is Ohno's postulate (*71*) that mammalian genomes consist of oases of genes in otherwise essentially empty deserts? It appears that the human genome does indeed contain deserts, or large, gene-poor regions. If we define a desert as a region >500 kbp without a gene, then we see that 605 Mbp, or about 20% of the genome, is in deserts. These are not uniformly distributed over the various chromosomes. Gene-rich chromosomes 17, 19, and 22 have only about 12% of their collective 171 Mbp in deserts, whereas gene-poor chromosomes 4, 13, 18, and X have 27.5% of their 492 Mbp in deserts (Table 11). The apparent lack of predicted genes in these regions does not necessarily imply that they are devoid of biological function.

4.2 Linkage map

Linkage maps provide the basis for genetic analysis and are widely used in the study of the inheritance of traits and in the positional cloning of genes. The distance metric, centimorgans (cM), is based on the recombination rate between homologous chromosomes during meiosis. In general, the rate of recombination in females is greater than that in males, and this degree of map expansion is not uniform across the genome (*72*). One of the opportunities enabled by a nearly complete genome sequence is to produce the ultimate physical map, and to fully analyze its correspondence with two other maps that have been widely used in genome and genetic analysis: the linkage map and the cytogenetic map. This would close the loop between the mapping and sequencing phases of the genome project.

We mapped the location of the markers that constitute the Genethon linkage map to the genome. The rate of recombination, expressed as cM per Mbp, was calculated for 3-Mbp windows as shown in Table 12. Higher rates of recombination in the telomeric region of the chromosomes have been previously documented (*73*). From this mapping result, there is a difference of 4.99 between lowest rates and highest rates and the largest difference of 4.4 between males and females (4.99 to 0.47 on chromosome 16). This indicates that the variability in recombination rates among regions of the genome exceeds the differences in recombination rates between males and females. The human genome has recombination hotspots, where recombination rates vary fivefold or more over a space of 1 kbp, so the picture one gets of the magnitude of variability in recombination rate will depend on the size of the window

Table 9. Characteristics of G+C in isochores.

Isochore	G+C (%)	Fraction of genome		Fraction of genes	
		Predicted*	Observed	Predicted*	Observed
H3	>48	5	9.5	37	24.8
H1/H2	43–48	25	21.2	32	26.6
L	<43	67	69.2	31	48.5

*The predictions were based on Bernardi's definitions (*70*) of the isochore structure of the human genome.

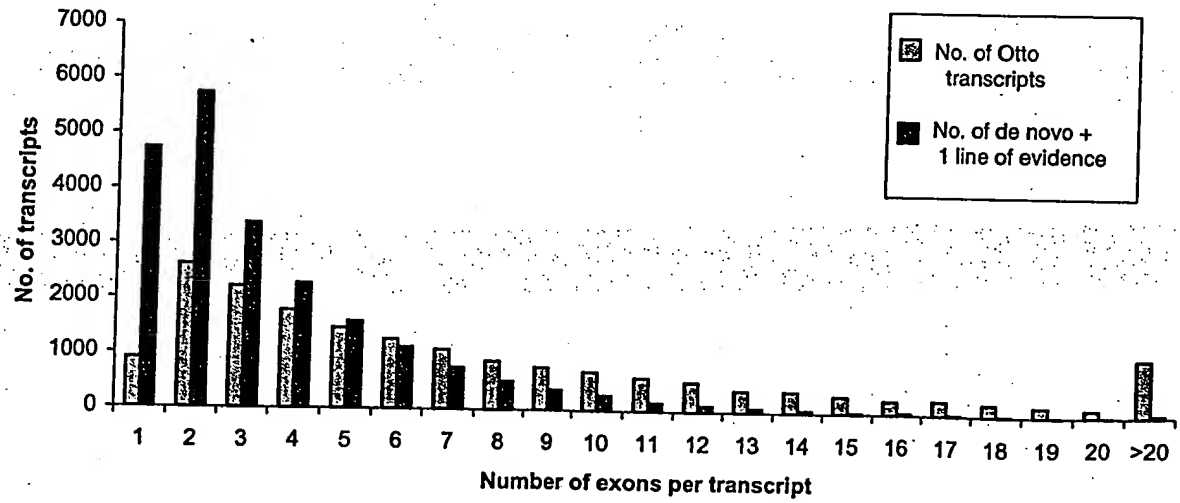

Fig. 9. Comparison of the number of exons per transcript between the 17,968 Otto transcripts and 21,350 de novo transcript predictions with at least one line of evidence that do not overlap with an Otto prediction. Both sets have the highest number of transcripts in the two-exon category, but the de novo gene predictions are skewed much more toward smaller transcripts. In the Otto set, 19.7% of the transcripts have one or two exons, and 5.7% have more than 20. In the de novo set, 49.3% of the transcripts have one or two exons, and 0.2% have more than 20.

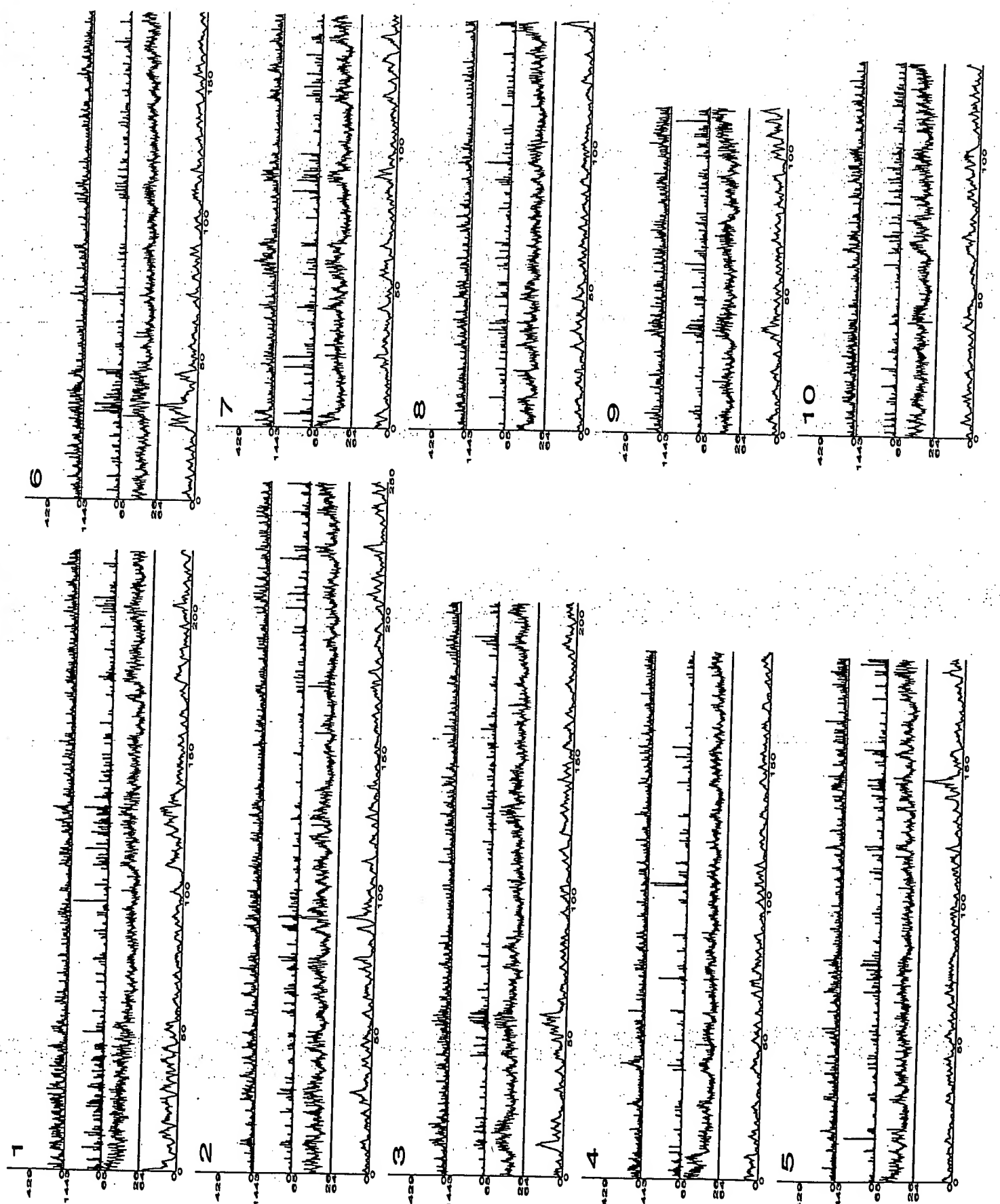

Fig. 11. Genome structural features.

Table 10. Features of the chromosomes. De novo/any refers to the union of de novo predictions that do not overlap Otto predictions and have at least one other type of supporting evidence; de novo/2x refers to the union of de novo predictions that do not overlap Otto predictions and have at least two types of evidence. Deserts are regions of sequence with no annotated genes.

	Sequence coverage (CS assembly)						Base composition			Gene prediction*					Gene density (genes/Mbp)						
Chr.	Size (Mbp)	No. of scaffolds	Largest scaffold (Mbp)	No. of scaffolds >500 kbp	Sequence covered by scaffolds >500 kbp	% of total sequence in scaffolds >500 kbp	% repeat	% GC	No of CpG islands	Otto	De novo/ any	De novo/ 2×	Total (Otto + de novo/ any)	Total (Otto + de novo/ any)	Sequence in deserts >500/ kbp	Sequence in deserts >1 Mbp	Otto	De novo/ any	De novo/ 2×	Otto + de novo/ any	Otto + de novo/ 2×
1	220	2,549	11	82	192	88	37	42	2,335	1,743	1,710	710	3,453	2,453	29	6	8	8	3	16	11
2	240	3,263	13	78	217	91	36	40	1,703	1,183	1,771	633	2,954	1,816	55	19	5	7	2	12	7
3	200	3,532	7	78	173	87	37	40	1,271	1,013	1,414	598	2,427	1,611	50	12	5	7	3	12	8
4	186	2,180	10	70	169	91	37	38	1,081	696	1,165	449	1,861	1,145	55	18	4	6	2	10	6
5	182	3,231	11	63	163	89	37	40	1,302	892	1,244	474	2,136	1,366	46	15	5	7	2	11	7
6	172	1,713	13	58	160	93	37	40	1,384	943	1,314	524	2,257	1,467	38	9	6	7	3	13	8
7	146	1,326	14	53	130	89	38	40	1,406	759	1,072	460	1,831	1,219	26	12	5	7	3	12	8
8	146	1,772	11	54	135	92	36	40	948	583	977	357	1,560	940	33	6	4	7	2	11	6
9	113	1,616	8	40	101	89	38	41	1,315	689	848	329	1,537	1,018	22	9	6	7	3	13	8
10	130	2,005	9	55	116	89	36	42	1,087	685	968	342	1,653	1,027	21	8	5	7	2	12	7
11	132	2,814	9	44	116	88	39	42	1,461	1,051	1,134	535	2,185	1,586	27	9	8	8	4	16	12
12	134	2,614	8	51	117	87	38	41	1,131	925	936	417	1,861	1,342	24	9	7	7	3	14	10
13	99	1,038	13	34	91	91	36	38	644	341	691	241	1,032	582	31	16	4	7	2	10	5
14	87	576	11	16	83	95	40	41	913	583	700	290	1,283	873	34	20	7	8	3	14	10
15	80	1,747	8	31	70	87	37	42	722	558	640	246	1,198	804	8	1	7	8	3	15	10
16	75	1,520	8	27	62	82	40	44	1,533	748	673	247	1,421	995	13	3	10	9	3	19	12
17	78	1,683	6	40	61	78	39	45	1,489	897	648	313	1,545	1,210	15	6	12	8	4	19	15
18	79	1,333	13	18	72	92	36	40	510	283	543	189	826	472	21	10	4	7	2	10	6
19	58	2,282	3	31	38	67	57	49	2,804	1,141	534	268	1,675	1,409	3	0	20	9	4	29	23
20	61	580	14	17	58	94	41	44	997	517	469	180	986	697	7	1	8	7	3	16	11
21	33	358	10	6	32	96	38	41	519	184	265	102	449	286	15	9	6	8	3	13	8
22	36	333	11	12	32	88	44	48	1,173	494	341	147	835	641	3	0	14	9	4	23	17
X	128	1,346	4	91	93	73	46	39	726	605	860	387	1,465	992	29	8	5	6	3	11	7
Y	19	638	2	10	12	65	50	39	65	55	155	49	210	104	4	2	3	8	2	11	5
U*	75	11,542	1						479	196	278	132	474	328							
Total	2907	53,591		1,059	2,490				28,519	17,764	21,350	8,619	39,114	26,383	606	208					
Avg.	116	2,144	9	44	104	87	40	41	1,160	714	812	333	1,526	1,047	25	9	7	7	3	14	9

*Chromosomal assignment unknown.

that account for gene inactivation. The general structural characteristics of these processed pseudogenes include the complete lack of intervening sequences found in the functional counterparts, a poly(A) tract at the 3′ end, and direct repeats flanking the pseudogene sequence. Processed pseudogenes occur as a result of retrotransposition, whereas unprocessed pseudogenes arise from segmental genome duplication.

We searched the complete set of Otto-predicted transcripts against the genomic sequence by means of BLAST. Genomic regions corresponding to all Otto-predicted transcripts were excluded from this analysis. We identified 2909 regions matching with greater than 70% identity over at least 70% of the length of the transcripts that likely represent processed pseudogenes. This number is probably an underestimate because specific methods to search for pseudogenes were not used.

We looked for correlations between structural elements and the propensity for retrotransposition in the human genome. GC content and transcript length were compared between the genes with processed pseudogenes (1177 source genes) versus the remainder of the predicted gene set. Transcripts that give rise to processed pseudogenes have shorter average transcript length (1027 bp versus 1594 bp for the Otto set) as compared with genes for which no pseudogene was detected. The overall GC content did not show any significant difference, contrary to a recent report (*88*). There is a clear trend in gene families that are present as processed pseudogenes. These include ribosomal proteins (67%), lamin receptors (10%), translation elongation factor alpha (5%), and HMG–non-histone proteins (2%). The increased occurrence of retrotransposition (both intronless paralogs and processed pseudogenes) among genes involved in translation and nuclear regulation may reflect an increased transcriptional activity of these genes.

5.3 Gene duplication in the human genome

Building on a previously published procedure (*27*), we developed a graph-theoretic algorithm, called Lek, for grouping the predicted human protein set into protein families (*89*).

Table 13. Characteristics of CpG islands identified in chromosome 22 (34-Mbp sequence length) and the whole genome (2.9-Gbp sequence length) by means of two different methods. Method 1 uses a CG likelihood ratio of ≥0.6. Method 2 uses a CG likelihood ratio of ≥0.8.

	Chromosome 22		Whole genome (CS assembly)	
	Method 1	Method 2	Method 1	Method 2
Number of CpG islands detected	5,211	522	195,706	26,876
Average length of island (bp)	390	535	395	497
Percent of sequence predicted as CpG	5.9	0.8	2.6	0.4
Percent of first exons that overlap a CpG island	44	25	42	22
Percent of first exons with first position of exon contained inside a CpG island	37	22	40	21
Average distance between first exon and closest CpG island (bp)	1,013	10,486	2,182	17,021
Expected distance between first exon and closest CpG island (bp)	3,262	32,567	7,164	55,811

Table 14. Distribution of repetitive DNA in the compartmentalized shotgun assembly sequence.

Repetitive elements	Megabases in assembled sequences	Percent of assembly	Previously predicted (%) (*83*)
Alu	288	9.9	10.0
Mammalian interspersed repeat (MIR)	66	2.3	1.7
Medium reiteration (MER)	50	1.7	1.6
Long terminal repeat (LTR)	155	5.3	5.6
Long interspersed nucleotide element (LINE)	466	16.1	16.7
Total	1025	35.3	35.6

The complete clusters that result from the Lek clustering provide one basis for comparing the role of whole-genome or chromosomal duplication in protein family expansion as opposed to other means, such as tandem duplication. Because each complete cluster represents a closed and certain island of homology, and because Lek is capable of simultaneously clustering protein complements of several organisms, the number of proteins contributed by each organism to a complete cluster can be predicted with confidence depending on the quality of the annotation of each genome. The variance of each organism's contribution to each cluster can then be calculated, allowing an assessment of the relative importance of large-scale duplication versus smaller-scale, organism-specific expansion and contraction of protein families, presumably as a result of natural selection operating on individual protein families within an organism. As can be seen in Fig. 12, the large variance in the relative numbers of human as compared with *D. melanogaster* and *Caenorhabditis elegans* proteins in complete clusters may be explained by multiple events of relative expansions in gene families in each of the three animal genomes. Such expansions would give rise to the distribution that shows a peak at 1:1 in the ratio for human-worm or human-fly clusters with the slope spread covering both human and fly/worm predominance, as we observed (Fig. 12). Furthermore, there are nearly as many clusters where worm and fly proteins predominate despite the larger numbers of proteins in the human. At face value, this analysis suggests that natural selection acting on individual protein families has been a major force driving the expansion of at least some elements of the human protein set. However, in our analysis, the difference between an ancient whole-genome duplication followed by loss, versus piecemeal duplication, cannot be easily distinguished. In order to differentiate these scenarios, more extended analyses were performed.

5.4 Large-scale duplications

Using two independent methods, we searched for large-scale duplications in the human genome. First, we describe a protein family–based method that identified highly conserved blocks of duplication. We then describe our comprehensive method for identifying all interchromosomal block duplications. The latter method identified a large number of duplicated chromosomal segments covering parts of all 24 chromosomes.

The first of the methods is based on the idea of searching for blocks of highly conserved homologous proteins that occur in more than one location on the genome. For this comparison, two genes were considered equivalent if their protein products were de-

By this measure, the duplication segment spans nearly half of each chromosome's net length. The most likely scenario is that the whole span of this region was duplicated as a single very large block, followed by shuffling owing to smaller scale rearrangements. As such, at least four subsequent rearrangements would need to be invoked to explain the relative insertions and inversions seen in the duplicated segment interval. The 64 protein pairs in this alignment occur among 217 protein assignments on chromosome 18, and among 322 protein assignments on chromosome 20, for a density of involved proteins of 20 to 30%. This is consistent with an ancient large-scale duplication followed by subsequent gene loss on one or both chromosomes. Loss of just one member of a gene pair subsequent to the duplication would result in a failure to score a gene pair in the block; less than 50% gene loss on the chromosomes would lead to the duplication density observed here. As an independent verification of the significance of the alignments detected, it can be seen that a substantial number of the pairs of aligning proteins in this duplication, including some of those annotated (Fig. 13), are those populating small Lek complete clusters (see above). This indicates that they are members of very small families of paralogs; their relative scarcity within the genome validates the uniqueness and robust nature of their alignments.

Two additional qualitative features were observed among many of the large-scale duplications. First, several proteins with disease associations, with OMIM (Online Mendelian Inheritance in Man) assignments, are members of duplicated segments (see web table 2 on *Science* Online at www.sciencemag.org/cgi/content/full/291/5507/1304/DC1). We have also observed a few instances where paralogs on both duplicated segments are associated with similar disease conditions. Notable among these genes are proteins involved in hemostasis (coagulation factors) that are associated with bleeding disorders, transcriptional regulators like the homeobox proteins associated with developmental disorders, and potassium channels associated with cardiovascular conduction abnormalities. For each of these disease genes, closer study of the paralogous genes in the duplicated segment may reveal new insights into disease causation, with further investigation needed to determine whether they might be involved in the same or similar genetic diseases. Second, although there is a conserved number of proteins and coding exons predicted for specific large duplicated spans within the chromosome 18 to 20 alignment, the genomic DNA of chromosome 18 in these specific spans is in some cases more than 10-fold longer than the corresponding chromosome 20 DNA. This selective accretion of noncoding DNA (or conversely, loss of noncoding DNA) on one of a pair of duplicated chromosome regions was observed in many compared regions. Hypotheses to explain which mechanisms foster these processes must be tested.

Evaluation of the alignment results gives some perspective on dating of the duplications. As noted above, large-scale ancient segmental duplication in fact best explains many of the blocks detected by this genome-wide analysis. The regions of human chromosomes involved in the large-scale duplications expanded upon above (chromosomes 2 to 14, 2 to 12, and 18 to 20) are each syntenic to a distinct mouse chromosomal region. The corresponding mouse chromosomal regions are much more similar in sequence conservation, and even in order, to their human synteny partners than the human duplication regions are to each other. Further, the corresponding mouse chromosomal regions each bear a significant proportion of genes orthologous to the human genes on which the human duplication assignments were made. On the basis of these factors, the corresponding mouse chromosomal spans, at coarse resolution, appear to be products of the same large-scale duplications observed in humans. Although further detailed analysis must be carried out once a more complete genome is assembled for mouse, the underlying large duplications appear to predate the two species' divergence. This dates the duplications, at the latest, before divergence of the primate and rodent lineages. This date can be further refined upon examination of the synteny between human chromosomes and those of chicken, pufferfish (*Fugu rubripes*), or zebrafish (*95*). The only substantial syntenic stretches mapped in these species corresponding to both pairs of human duplications are restricted to the Hox cluster regions. When the synteny of these regions (or others) to human chromosomes is extended with further mapping, the ages of the nearly chromosome-length duplications seen in humans are likely to be dated to the root of vertebrate divergence.

The MUMmer-based results demonstrate large block duplications that range in size from a few genes to segments covering most of a chromosome. The extent of segmental duplications raises the question of whether an ancient whole-genome duplication event is the underlying explanation for the numerous duplicated regions (*96*). The duplications have undergone many deletions and subsequent rearrangements; these events make it difficult to distinguish between a whole-genome duplication and multiple smaller events. Further analysis, focused especially on comparing the estimated ages of all the block duplications, derived partially from interspecies genome comparisons, will be necessary to determine which of these two hypotheses is more likely. Comparisons of genomes of different vertebrates, and even cross-phyla genome comparisons, will allow for the deconvolution of duplications to eventually reveal the stagewise history of our genome, and with it a history of the emergence of many of the key functions that distinguish us from other living things.

6 A Genome-Wide Examination of Sequence Variations

Summary. Computational methods were used to identify single-nucleotide polymorphisms (SNPs) by comparison of the Celera sequence to other SNP resources. The SNP rate between two chromosomes was ~1 per 1200 to 1500 bp. SNPs are distributed nonrandomly throughout the genome. Only a very small proportion of all SNPs (<1%) potentially impact protein function based on the functional analysis of SNPs that affect the predicted coding regions. This results in an estimate that only thousands, not millions, of genetic variations may contribute to the structural diversity of human proteins.

Having a complete genome sequence enables researchers to achieve a dramatic acceleration in the rate of gene discovery, but only through analysis of sequence variation in DNA can we discover the genetic basis for variation in health among human beings. Whole-genome shotgun sequencing is a particularly effective method for detecting sequence variation in tandem with whole-genome assembly. In addition, we compared the distribution and attributes of SNPs ascertained by three other methods: (i) alignment of the Celera consensus sequence to the PFP assembly, (ii) overlap of high-quality reads of genomic sequence (referred to as "Kwok"; 1,120,195 SNPs) (*97*), and (iii) reduced representation shotgun sequencing (referred to as "TSC"; 632,640 SNPs) (*98*). These data were consistent in showing an overall nucleotide diversity of ~8×10^{-4}, marked heterogeneity across the genome in SNP density, and an overwhelming preponderance of noncoding variation that produces no change in expressed proteins.

6.1 SNPs found by aligning the Celera consensus to the PFP assembly

Ideally, methods of SNP discovery make full use of sequence depth and quality at every site, and quantitatively control the rate of false-positive and false-negative calls with an explicit sampling model (*99*). Comparison of consensus sequences in the absence of these details necessitated a more ad hoc approach (quality scores could not readily be obtained for the PFP assembly). First, all sequence differences between the two consensus sequences were identified; these were then filtered to reduce the contribution of sequencing errors and misassembly. As a measure of the effectiveness of the filtering step, we monitored the ratio of transition and transversion substitutions, because a 2:1 ratio has been well documented as typical in mammalian evolution (*100*) and in human SNPs

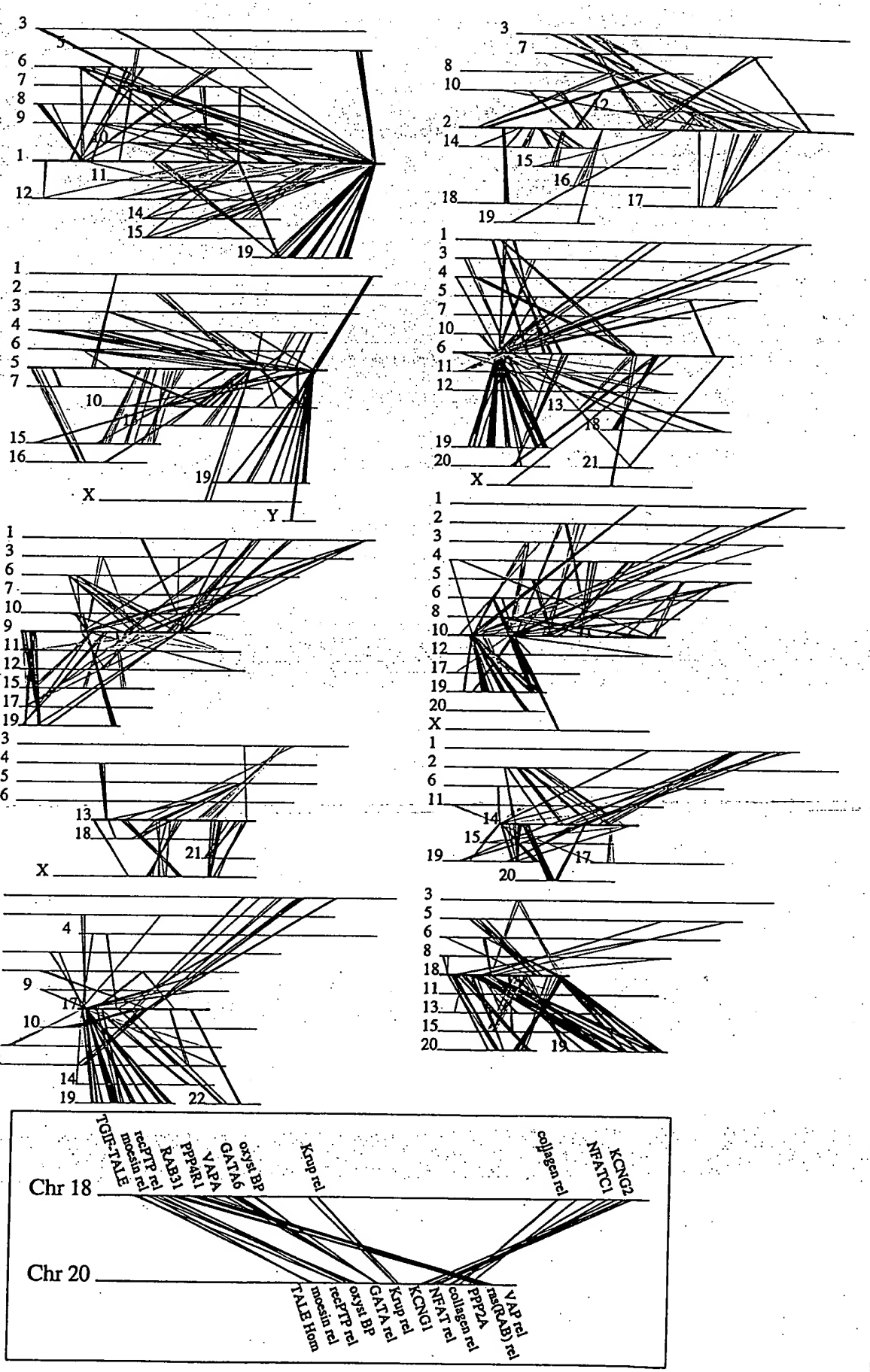

Fig. 13. Segmental duplications between chromosomes in the human genome. The 24 panels show the 1077 duplicated blocks of genes, containing 10,310 pairs of genes in total. Each line represents a pair of homologous genes belonging to a block; all blocks contain at least three genes on each of the chromosomes where they appear. Each panel shows all the duplications between a single chromosome and other chromosomes with shared blocks. The chromosome at the center of each panel is shown as a thick red line for emphasis. Other chromosomes are displayed from top to bottom within each panel ordered by chromosome number. The inset (bottom, center right) shows a close-up of one duplication between chromosomes 18 and 20, expanded to display the gene names of 12 of the 64 gene pairs shown.

somes, and whether this heterogeneity is greater than expected by chance. If SNPs occur by random and independent mutations, then it would seem that there ought to be a Poisson distribution of numbers of SNPs in fragments of arbitrary constant size. The observed dispersion in the distribution of SNPs in 100-kbp fragments was far greater than predicted from a Poisson distribution (Fig. 14). However, this simplistic model ignores the different recombination rates and population histories that exist in different regions of the genome. Population genetics theory holds that we can account for this variation with a mathematical formulation called the neutral coalescent (*109*). Applying well-tested algorithms for simulating the neutral coalescent with recombination (*110*), and using an effective population size of 10,000 and a per-base recombination rate equal to the mutation rate (*111*), we generated a distribution of numbers of SNPs by this model as well (*112*). The observed distribution of SNPs has a much larger variance than either the Poisson model or the coalescent model, and the difference is highly significant. This implies that there is significant variability across the genome in SNP density, an observation that begs an explanation.

Several attributes of the DNA sequence may affect the local density of SNPs, including the rate at which DNA polymerase makes errors and the efficacy of mismatch repair. One key factor that is likely to be associated with SNP density is the G+C content, in part because methylated cytosines in CpG dinucleotides tend to undergo deamination to form thymine, accounting for a nearly 10-fold increase in the mutation rate of CpGs over other dinucleotides. We tallied the GC content and nucleotide diversities in 100-kbp windows across the entire genome and found that the correlation between them was positive ($r = 0.21$) and highly significant ($P < 0.0001$), but G+C content accounted for only a small part of the variation.

6.5 SNPs by genomic class

To test homogeneity of SNP densities across functional classes, we partitioned sites into intergenic (defined as >5 kbp from any predicted transcription unit), 5′-UTR, exonic (missense and silent), intronic, and 3′-UTR for 10,239 known genes, derived from the NCBI RefSeq database and all human genes predicted from the Celera Otto annotation. In coding regions, SNPs were categorized as either silent, for those that do not change amino acid sequence, or missense, for those that change the protein product. The ratio of missense to silent coding SNPs in Celera-PFP, TSC, and Kwok sets (1.12, 0.91, and 0.78, respectively) shows a markedly reduced frequency of missense variants compared with the neutral expectation, consistent with the elimination by natural selection of a fraction of the deleterious amino acid changes (*112*). These ratios are comparable to the missense-to-silent ratios of 0.88 and 1.17 found by Cargill *et al.* (*101*) and by Halushka *et al.* (*102*). Similar results were observed in SNPs derived from Celera shotgun sequences (*46*).

It is striking how small is the fraction of SNPs that lead to potentially dysfunctional alterations in proteins. In the 10,239 RefSeq genes, missense SNPs were only about 0.12, 0.14, and 0.17% of the total SNP counts in Celera-PFP, TSC, and Kwok SNPs, respectively. Nonconservative protein changes constitute an even smaller fraction of missense SNPs (47, 41, and 40% in Celera-PFP, Kwok, and TSC). Intergenic regions have been virtually unstudied (*113*), and we note that 75% of the SNPs we identified were intergenic (Table 17). The SNP rate was highest in introns and lowest in exons. The SNP rate was lower in intergenic regions than in introns, providing one of the first discriminators between these two classes of DNA. These SNP rates were confirmed in the Celera SNPs, which also exhibited a lower rate in exons than in introns, and in extragenic regions than in introns (*46*). Many of these intergenic SNPs will provide valuable information in the form of markers for linkage and association studies, and some fraction is likely to have a regulatory function as well.

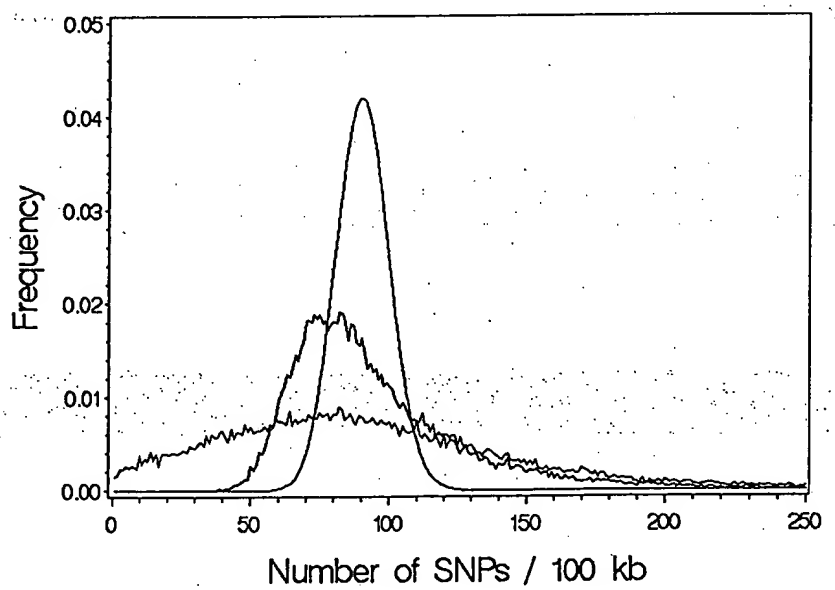

Fig. 14. SNP density in each 100-kbp interval as determined with Celera-PFP SNPs. The color codes are as follows: black, Celera-PFP SNP density; blue, coalescent model; and red, Poisson distribution. The figure shows that the distribution of SNPs along the genome is nonrandom and is not entirely accounted for by a coalescent model of regional history.

7 An Overview of the Predicted Protein-Coding Genes in the Human Genome

Summary. This section provides an initial computational analysis of the predicted protein set with the aim of cataloging prominent differences and similarities when the human genome is compared with other fully sequenced eukaryotic genomes. Over 40% of the predicted protein set in humans cannot be ascribed a molecular function by methods that assign proteins to known families. A protein domain–based analysis provides a detailed catalog of the prominent differences in the human genome when compared with the fly and worm genomes. Prominent among these are domain expansions in proteins involved in developmental regulation and in cellular processes such as neuronal function, hemostasis, acquired immune response, and cytoskeletal complexity. The final enumeration of protein families and details of protein structure will rely on additional experimental work and comprehensive manual curation.

A preliminary analysis of the predicted human protein-coding genes was conducted. Two methods were used to analyze and classify the molecular functions of 26,588 predicted proteins that represent 26,383 gene predictions with at least two lines of evidence as described above. The first method was based on an analysis at the level of protein families, with both the publicly available Pfam database (*114*, *115*) and Celera's Panther Classification (CPC) (Fig. 15) (*116*). The second method was based on an analysis at the level of protein domains, with both the Pfam and SMART databases (*115*, *117*).

The results presented here are preliminary and are subject to several limitations.

7.2 Evolutionary conservation of core processes

Because of the various "model organism" genome-sequencing projects that have already been completed, reasonable comparative information is available for beginning the analysis of the evolution of the human genome. The genomes of *S. cerevisiae* ("bakers' yeast") (*118*) and two diverse invertebrates, *C. elegans* (a nematode worm) (*119*) and *D. melanogaster* (fly) (*26*), as well as the first plant genome, *A. thaliana*, recently completed (*92*), provide a diverse background for genome comparisons.

We enumerated the "strict orthologs" conserved between human and fly, and between human and worm (Fig. 16) to address the question, What are the core functions that appear to be common across the animals? The concept of orthology is important because if two genes are orthologs, they can be traced by descent to the common ancestor of the two organisms (an "evolutionarily conserved protein set"), and therefore are likely to perform similar conserved functions in the different organisms. It is critical in this analysis to separate orthologs (a gene that appears in two organisms by descent from a common ancestor) from paralogs (a gene that appears in more than one copy in a given organism by a duplication event) because paralogs may subsequently diverge in function. Following the yeast-worm ortholog comparison in (*120*), we identified two different cases for each pairwise comparison (human-fly and human-worm). The first case was a pair of genes, one from each organism, for which there was no other close homolog in either organism. These are straightforwardly identified as orthologous, because there are no additional members of the families that complicate separating orthologs from paralogs. The second case is a family of genes with more than one member in either or both of the organisms being compared. Chervitz *et al.* (*120*) deal with this case by analyzing a phylogenetic tree that described the relationships between all of the sequences in both organisms, and then looked for pairs of genes that were nearest neighbors in the tree. If the nearest-neighbor pairs were from different organisms, those genes were presumed to be orthologs. We note that these nearest neighbors can often be confidently identified from pairwise sequence comparison without having to examine a phylogenetic tree (see legend to Fig. 16). If the nearest neighbors are not from different organisms, there has been a paralogous expansion in one or both organisms after the speciation event (and/or a gene loss by one organism). When this one-to-one correspondence is lost, defining an ortholog becomes ambiguous. For our initial computational overview of the predicted human protein set, we could not answer this question for every predicted protein. Therefore, we consider only "strict orthologs," i.e., the proteins with unambiguous one-to-one relationships (Fig. 16). By these criteria, there are 2758 strict human-fly orthologs, 2031 human-worm (1523 in common between these sets). We define the evolutionarily conserved set as those 1523 human proteins that have strict orthologs in both *D. melanogaster* and *C. elegans*.

The distribution of the functions of the conserved protein set is shown in Fig. 16. Comparison with Fig. 15 shows that, not surprisingly, the set of conserved proteins is not distributed among molecular functions in the same way as the whole human protein set. Compared with the whole human set (Fig. 15), there are several categories that are overrepresented in the conserved set by a factor of ~2 or more. The first category is nucleic acid enzymes, primarily the transcriptional machinery (notably DNA/RNA methyltransferases, DNA/RNA polymerases, helicases, DNA ligases, DNA- and RNA-processing factors, nucleases, and ribosomal proteins). The basic transcriptional and translational machinery is well known to have been conserved over evolution, from bacteria through to the most complex eukaryotes. Many ribonucleoproteins involved in RNA splicing also appear to be conserved among the animals. Other enzyme types are also overrepresented (transferases, oxidoreductases, ligases, lyases, and isomerases). Many of these en-

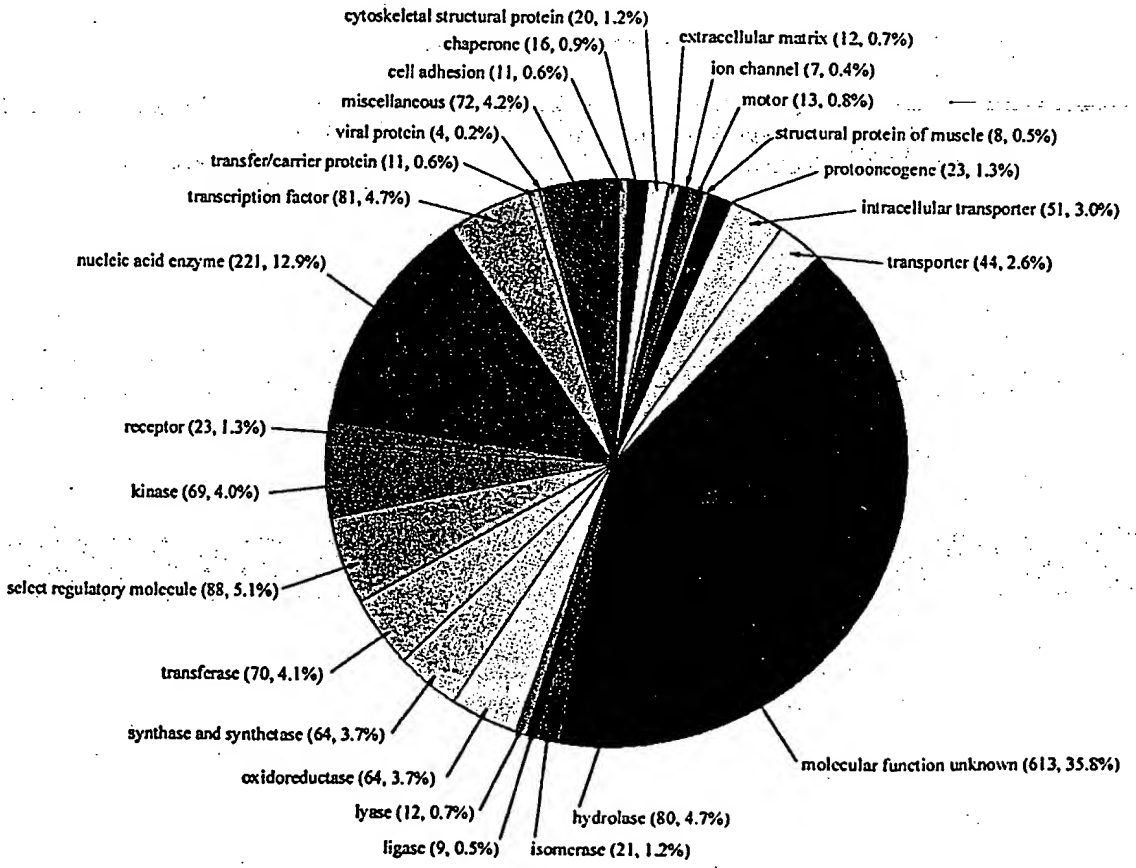

Fig. 16. Functions of putative orthologs across vertebrate and invertebrate genomes. Each slice lists the number and percentages (in parentheses) of "strict orthologs" between the human, fly, and worm genomes involved in a given category of molecular function. "Strict orthologs" are defined here as bi-directional BLAST best hits (*180*) such that each orthologous pair (i) has a BLASTP *P*-value of $\leq 10^{-10}$ (*120*), and (ii) has a more significant BLASTP score than any paralogs in either organism, i.e., there has likely been no duplication subsequent to speciation that might make the orthology ambiguous. This measure is quite strict and is a lower bound on the number of orthologs. By these criteria, there are 2758 strict human-fly orthologs, and 2031 human-worm orthologs (1523 in common between these sets).

Table 18. Domain-based comparative analysis of proteins in *H. sapiens* (H), *D. melanogaster* (F), *C. elegans* (W), *S. cerevisiae* (Y), and *A. thaliana* (A). The predicted protein set of each of the above eukaryotic organisms was analyzed with Pfam version 5.5 using E value cutoffs of 0.001. The number of proteins containing the specified Pfam domains as well as the total number of domains (in parentheses) are shown in each column. Domains were categorized into cellular processes for presentation. Some domains (i.e., SH2) are listed in more than one cellular process. Results of the Pfam analysis may differ from results obtained based on human curation of protein families, owing to the limitations of large-scale automatic classifications. Representative examples of domains with reduced counts owing to the stringent E value cutoff used for this analysis are marked with a double asterisk (**). Examples include short divergent and predominantly alpha-helical domains, and certain classes of cysteine-rich zinc finger proteins.

Accession number	Domain name	Domain description	H	F	W	Y	A
		Developmental and homeostatic regulators					
PF02039	Adrenomedullin	Adrenomedullin	1	0	0	0	0
PF00212	ANP	Atrial natriuretic peptide	2	0	0	0	0
PF00028	Cadherin	Cadherin domain	100 (550)	14 (157)	16 (66)	0	0
PF00214	Calc_CGRP_IAPP	Calcitonin/CGRP/IAPP family	3	0	0	0	0
PF01110	CNTF	Ciliary neurotrophic factor	1	0	0	0	0
PF01093	Clusterin	Clusterin	3	0	0	0	0
PF00029	Connexin	Connexin	14 (16)	0	0	0	0
PF00976	ACTH_domain	Corticotropin ACTH domain	1	0	0	0	0
PF00473	CRF	Corticotropin-releasing factor family	2	1	0	0	0
PF00007	Cys_knot	Cystine-knot domain	10 (11)	2	0	0	0
PF00778	DIX	Dix domain	5	2	4	0	0
PF00322	Endothelin	Endothelin family	3	0	0	0	0
PF00812	Ephrin	Ephrin	7 (8)	2	4	0	0
PF01404	EPh_lbd	Ephrin receptor ligand binding domain	12	2	1	0	0
PF00167	FGF	Fibroblast growth factor	23	1	1	0	0
PF01534	Frizzled	Frizzled/Smoothened family membrane region	9	7	3	0	0
PF00236	Hormone6	Glycoprotein hormones	1	0	0	0	0
PF01153	Glypican	Glypican	14	2	1	0	0
PF01271	Granin	Grainin (chromogranin or secretogranin)	3	0	0	0	0
PF02058	Guanylin	Guanylin precursor	1	0	0	0	0
PF00049	Insulin	Insulin/IGF/Relaxin family	7	4	0	0	0
PF00219	IGFBP	Insulin-like growth factor binding proteins	10	0	0	0	0
PF02024	Leptin	Leptin	1	0	0	0	0
PF00193	Xlink	LINK (hyaluron binding)	13 (23)	0	1	0	0
PF00243	NGF	Nerve growth factor family	3	0	0	0	0
PF02158	Neuregulin	Neuregulin family	4	0	0	0	0
PF00184	Hormone5	Neurohypophysial hormones	1	0	0	0	0
PF02070	NMU	Neuromedin U	1	0	0	0	0
PF00066	Notch	Notch (DSL) domain	3 (5)	2 (4)	2 (6)	0	0
PF00865	Osteopontin	Osteopontin	1	0	0	0	0
PF00159	Hormone3	Pancreatic hormone peptides	3	0	0	0	0
PF01279	Parathyroid	Parathyroid hormone family	2	0	0	0	0
PF00123	Hormone2	Peptide hormone	5 (9)	0	0	0	0
PF00341	PDGF	Platelet-derived growth factor (PDGF)	5	1	0	0	0
PF01403	Sema	Sema domain	27 (29)	8 (10)	3 (4)	0	0
PF01033	Somatomedin_B	Somatomedin B domain	5 (8)	3	0	0	0
PF00103	Hormone	Somatotropin	1	0	0	0	0
PF02208	Sorb	Sorbin homologous domain	2	0	0	0	0
PF02404	SCF	Stem cell factor	2	0	0	0	0
PF01034	Syndecan	Syndecan domain	3	1	1	0	0
PF00020	TNFR_c6	TNFR/NGFR cysteine-rich region	17 (31)	1	0	0	0
PF00019	TGF-β	Transforming growth factor β-like domain	27 (28)	6	4	0	0
PF01099	Uteroglobin	Uteroglobin family	3	0	0	0	0
PF01160	Opiods_neuropep	Vertebrate endogenous opioids neuropeptide	3	0	0	0	0
PF00110	Wnt	Wnt family of developmental signaling proteins	18	7 (10)	5	0	0
		Hemostasis					
PF01821	ANATO	Anaphylotoxin-like domain	6 (14)	0	0	0	0
PF00386	C1q	C1q domain	24	0	0	0	0
PF00200	Disintegrin	Disintegrin	18	2	3	0	0
PF00754	F5_F8_type_C	F5/8 type C domain	15 (20)	5 (6)	2	0	0
PF01410	COLFI	Fibrillar collagen C-terminal domain	10	0	0	0	0
PF00039	Fn1	Fibronectin type I domain	5 (18)	0	0	0	0
PF00040	Fn2	Fibronectin type II domain	11 (16)	0	0	0	0
PF00051	Kringle	Kringle domain	15 (24)	2	2	0	0
PF01823	MACPF	MAC/Perforin domain	6	0	0	0	0
PF00354	Pentaxin	Pentaxin family	9	0	0	0	0
PF00277	SAA_proteins	Serum amyloid A protein	4	0	0	0	0
PF00084	Sushi	Sushi domain (SCR repeat)	53 (191)	11 (42)	8 (45)	0	0
PF02210	TSPN	Thrombospondin N-terminal–like domains	14	1	0	0	0
PF01108	Tissue_fac	Tissue factor	1	0	0	0	0
PF00868	Transglutamin_N	Transglutaminase family	6	1	0	0	0
PF00927	Transglutamin_C	Transglutaminase family	8	1	0	0	0

Table 18 (*Continued*)

Accession number	Domain name	Domain description	H	F	W	Y	A
PF00620	RhoGAP	RhoGAP domain	59	19	20	9	8
PF00621	RhoGEF	RhoGEF domain	46	23 (24)	18 (19)	3	0
PF00536	SAM	SAM domain (Sterile alpha motif)	29 (31)	15	8	3	6
PF01369	Sec7	Sec7 domain	13	5	5	5	9
PF00017	SH2	Src homology 2 (SH2) domain	87 (95)	33 (39)	44 (48)	1	3
PF00018	SH3	Src homology 3 (SH3) domain	143 (182)	55 (75)	46 (61)	23 (27)	4
PF01017	STAT	STAT protein	7	1	1 (2)	0	0
PF00790	VHS	VHS domain	4	2	4	4	8
PF00568	WH1	WH1 domain	7	2	2 (3)	1	0
		Domains involved in apoptosis					
PF00452	Bcl-2	Bcl-2	9	2	1	0	0
PF02180	BH4	Bcl-2 homology region 4	3	0	1	0	0
PF00619	CARD	Caspase recruitment domain	16	0	2	0	0
PF00531	Death	Death domain	16	5	7	0	0
PF01335	DED	Death effector domain	4 (5)	0	0	0	0
PF02179	BAG	Domain present in Hsp70 regulators	5 (8)	3	2	1	5
PF00656	ICE_p20	ICE-like protease (caspase) p20 domain	11	7	3	0	0
PF00653	BIR	Inhibitor of Apoptosis domain	8 (14)	5 (9)	2 (3)	1 (2)	0
		Cytoskeletal					
PF00022	Actin	Actin	61 (64)	15 (16)	12	9 (11)	24
PF00191	Annexin	Annexin	16 (55)	4 (16)	4 (11)	0	6 (16)
PF00402	Calponin	Calponin family	13 (22)	3	7 (19)	0	0
PF00373	Band_41	FERM domain (Band 4.1 family)	29 (30)	17 (19)	11 (14)	0	0
PF00880	Nebulin_repeat	Nebulin repeat	4 (148)	1 (2)	1	0	0
PF00681	Plectin_repeat	Plectin repeat	2 (11)	0	0	0	0
PF00435	Spectrin	Spectrin repeat	31 (195)	13 (171)	10 (93)	0	0
PF00418	Tubulin-binding	Tau and MAP proteins, tubulin-binding	4 (12)	1 (4)	2 (8)	0	0
PF00992	Troponin	Troponin	4	6	8	0	0
PF02209	VHP	Villin headpiece domain	5	2	2	0	5
PF01044	Vinculin	Vinculin family	4	2	1	0	0
		ECM adhesion					
PF01391	Collagen	Collagen triple helix repeat (20 copies)	65 (279)	10 (46)	174 (384)	0	0
PF01413	C4	C-terminal tandem repeated domain in type 4 procollagen	6 (11)	2 (4)	3 (6)	0	0
PF00431	CUB	CUB domain	47 (69)	9 (47)	43 (67)	0	0
PF00008	EGF	EGF-like domain	108 (420)	45 (186)	54 (157)	0	1
PF00147	Fibrinogen_C	Fibrinogen beta and gamma chains, C-terminal globular domain	26	10 (11)	6	0	0
PF00041	Fn3	Fibronectin type III domain	106 (545)	42 (168)	34 (156)	0	1
PF00757	Furin-like	Furin-like cysteine rich region	5	2	1	0	0
PF00357	Integrin_A	Integrin alpha cytoplasmic region	3	1	2	0	0
PF00362	Integrin_B	Integrins, beta chain	8	2	2	0	0
PF00052	Laminin_B	Laminin B (Domain IV)	8 (12)	4 (7)	6 (10)	0	0
PF00053	Laminin_EGF	Laminin EGF-like (Domains III and V)	24 (126)	9 (62)	11 (65)	0	0
PF00054	Laminin_G	Laminin G domain	30 (57)	18 (42)	14 (26)	0	0
PF00055	Laminin_Nterm	Laminin N-terminal (Domain VI)	10	6	4	0	0
PF00059	Lectin_c	Lectin C-type domain	47 (76)	23 (24)	91 (132)	0	0
PF01463	LRRCT	Leucine rich repeat C-terminal domain	69 (81)	23 (30)	7 (9)	0	0
PF01462	LRRNT	Leucine rich repeat N-terminal domain	40 (44)	7 (13)	3 (6)	0	0
PF00057	Ldl_recept_a	Low-density lipoprotein receptor domain class A	35 (127)	33 (152)	27 (113)	0	0
PF00058	Ldl_recept_b	Low-density lipoprotein receptor repeat class B	15 (96)	9 (56)	7 (22)	0	0
PF00530	SRCR	Scavenger receptor cysteine-rich domain	11 (46)	4 (8)	1 (2)	0	0
PF00084	Sushi	Sushi domain (SCR repeat)	53 (191)	11 (42)	8 (45)	0	0
PF00090	Tsp_1	Thrombospondin type 1 domain	41 (66)	11 (23)	18 (47)	0	0
PF00092	Vwa	von Willebrand factor type A domain	34 (58)	0	17 (19)	0	1
PF00093	Vwc	von Willebrand factor type C domain	19 (28)	6 (11)	2 (5)	0	0
PF00094	Vwd	von Willebrand factor type D domain	15 (35)	3 (7)	9	0	0
		Protein interaction domains					
PF00244	14-3-3	14-3-3 proteins	20	3	3	2	15
PF00023	Ank	Ank repeat	145 (404)	72 (269)	75 (223)	12 (20)	66 (111)
PF00514	Armadillo_seg	Armadillo/beta-catenin-like repeats	22 (56)	11 (38)	3 (11)	2 (10)	25 (67)
PF00168	C2	C2 domain	73 (101)	32 (44)	24 (35)	6 (9)	66 (90)
PF00027	cNMP_binding	Cyclic nucleotide-binding domain	26 (31)	21 (33)	15 (20)	2 (3)	22
PF01556	DnaJ_C	DnaJ C terminal region	12	9	5	3	19
PF00226	DnaJ	DnaJ domain	44	34	33	20	93
PF00036	Efhand**	EF hand	83 (151)	64 (117)	41 (86)	4 (11)	120 (328)
PF00611	FCH	Fes/CIP4 homology domain	9	3	2	4	0
PF01846	FF	FF domain	4 (11)	4 (10)	3 (16)	2 (5)	4 (8)
PF00498	FHA	FHA domain	13	15	7	13 (14)	17

Table 18 (*Continued*)

Accession number	Domain name	Domain description	H	F	W	Y	A
PF02135	Zf-TAZ	TAZ finger	2 (3)	1 (2)	6 (7)	0	10 (15)
PF01285	TEA	TEA domain	4	1	1	1	0
PF02176	Zf-TRAF	TRAF-type zinc finger	6 (9)	1 (3)	1	0	2
PF00352	TBP	Transcription factor TFIID (or TATA-binding protein, TBP)	2 (4)	4 (8)	2 (4)	1 (2)	2 (4)
PF00567	TUDOR	TUDOR domain	9 (24)	9 (19)	4 (5)	0	2
PF00642	Zf-CCCH	Zinc finger C-x8-C-x5-C-x3-H type (and similar)	17 (22)	6 (8)	22 (42)	3 (5)	31 (46)
PF00096	Zf-C2H2**	Zinc finger, C2H2 type	564 (4500)	234 (771)	68 (155)	34 (56)	21 (24)
PF00097	Zf-C3HC4	Zinc finger, C3HC4 type (RING finger)	135 (137)	57	88 (89)	18	298 (304)
PF00098	Zf-CCHC	Zinc knuckle	9 (17)	6 (10)	17 (33)	7 (13)	68 (91)

(Tables 18 and 19). They include secreted hormones and growth factors, receptors, intracellular signaling molecules, and transcription factors.

Developmental signaling molecules that are enriched in the human genome include growth factors such as wnt, transforming growth factor–β (TGF-β), fibroblast growth factor (FGF), nerve growth factor, platelet derived growth factor (PDGF), and ephrins. These growth factors affect tissue differentiation and a wide range of cellular processes involving actin-cytoskeletal and nuclear regulation. The corresponding receptors of these developmental ligands are also expanded in humans. For example, our analysis suggests at least 8 human ephrin genes (2 in the fly, 4 in the worm) and 12 ephrin receptors (2 in the fly, 1 in the worm). In the wnt signaling pathway, we find 18 wnt family genes (6 in the fly, 5 in the worm) and 12 frizzled receptors (6 in the fly, 5 in the worm). The Groucho family of transcriptional corepressors downstream in the wnt pathway are even more markedly expanded, with 13 predicted members in humans (2 in the fly, 1 in the worm).

Extracellular adhesion molecules involved in signaling are expanded in the human genome (Tables 18 and 19). The interactions of several of these adhesion domains with extracellular matrix proteoglycans play a critical role in host defense, morphogenesis, and tissue repair (*131*). Consistent with the well-defined role of heparan sulfate proteoglycans in modulating these interactions (*132*), we observe an expansion of the heparin sulfate sulfotransferases in the human genome relative to worm and fly. These sulfotransferases modulate tissue differentiation (*133*). A similar expansion in humans is noted in structural proteins that constitute the actin-cytoskeletal architecture. Compared with the fly and worm, we observe an explosive expansion of the nebulin (35 domains per protein on average), aggrecan (12 domains per protein on average), and plectin (5 domains per protein on average) repeats in humans. These repeats are present in proteins involved in modulating the actin-cytoskeleton with predominant expression in neuronal, muscle, and vascular tissues.

Comparison across the five sequenced eukaryotic organisms revealed several expanded protein families and domains involved in cytoplasmic signal transduction (Table 18). In particular, signal transduction pathways playing roles in developmental regulation and acquired immunity were substantially enriched. There is a factor of 2 or greater expansion in humans in the Ras superfamily GTPases and the GTPase activator and GTP exchange factors associated with them. Although there are about the same number of tyrosine kinases in the human and *C. elegans* genomes, in humans there is an increase in the SH2, PTB, and ITAM domains involved in phosphotyrosine signal transduction. Further, there is a twofold expansion of phosphodiesterases in the human genome compared with either the worm or fly genomes.

The downstream effectors of the intracellular signaling molecules include the transcription factors that transduce developmental fates. Significant expansions are noted in the ligand-binding nuclear hormone receptor class of transcription factors compared with the fly genome, although not to the extent observed in the worm (Tables 18 and 19). Perhaps the most striking expansion in humans is in the C2H2 zinc finger transcription factors. Pfam detects a total of 4500 C2H2 zinc finger domains in 564 human proteins, compared with 771 in 234 fly proteins. This means that there has been a dramatic expansion not only in the number of C2H2 transcription factors, but also in the number of these DNA-binding motifs per transcription factor (8 on average in humans, 3.3 on average in the fly, and 2.3 on average in the worm). Furthermore, many of these transcription factors contain either the KRAB or SCAN domains, which are not found in the fly or worm genomes. These domains are involved in the oligomerization of transcription factors and increase the combinatorial partnering of these factors. In general, most of the transcription factor domains are shared between the three animal genomes, but the reassortment of these domains results in organism-specific transcription factor families. The domain combinations found in the human, fly, and worm include the BTB with C2H2 in the fly and humans, and homeodomains alone or in combination with Pou and LIM domains in all of the animal genomes. In plants, however, a different set of transcription factors are expanded, namely, the myb family, and a unique set that includes VP1 and AP2 domain–containing proteins (*134*). The yeast genome has a paucity of transcription factors compared with the multicellular eukaryotes, and its repertoire is limited to the expansion of the yeast-specific C6 transcription factor family involved in metabolic regulation.

While we have illustrated expansions in a subset of signal transduction molecules in the human genome compared with the other eukaryotic genomes, it should be noted that most of the protein domains are highly conserved. An interesting observation is that worms and humans have approximately the same number of both tyrosine kinases and serine/threonine kinases (Table 19). It is important to note, however, that these are merely counts of the catalytic domain; the proteins that contain these domains also display a wide repertoire of interaction domains with significant combinatorial diversity.

Hemostasis. Hemostasis is regulated primarily by plasma proteases of the coagulation pathway and by the interactions that occur between the vascular endothelium and platelets. Consistent with known anatomical and physiological differences between vertebrates and invertebrates, extracellular adhesion domains that constitute proteins integral to hemostasis are expanded in the human relative to the fly and worm (Tables 18 and 19). We note the evolution of domains such as FIMAC, FN1, FN2, and C1q that mediate surface interactions between hematopoeitic cells and the vascular matrix. In addition, there has been extensive recruitment of more-ancient animal-specific domains such as VWA, VWC, VWD, kringle, and FN3 into multidomain proteins that are involved in hemostatic regulation. Although we do not find a large expansion in the total number of serine proteases, this enzymatic domain has been specifically recruited into several of these multidomain proteins for proteolytic regulation in the vascular compartment. These are represented in plasma proteins that belong to the kinin and complement pathways. There is a

alytic activity, as a uracil DNA glycosylase (*140*) and functions as a cell cycle regulator (*141*) and has even been implicated in apoptosis (*142*).

Translation. Another striking set of human expansions has occurred in certain families involved in the translational machinery. We identified 28 different ribosomal subunits that each have at least 10 copies in the genome; on average, for all ribosomal proteins there is about an 8- to 10-fold expansion in the number of genes relative to either the worm or fly. Retrotransposed pseudogenes may account for many of these expansions [see the discussion above and (*143*)]. Recent evidence suggests that a number of ribosomal proteins have secondary functions independent of their involvement in protein biosynthesis; for example, L13a and the related L7 subunits (36 copies in humans) have been shown to induce apoptosis (*144*).

There is also a four- to fivefold expansion in the elongation factor 1-alpha family (eEF1A; 56 human genes). Many of these expansions likely represent intronless paralogs that have presumably arisen from retrotransposition, and again there is evidence that many of these may be pseudogenes (*145*). However, a second form (eEF1A2) of this factor has been identied with tissue-specific expression in skeletal muscle and a complementary expression pattern to the ubiquitously expressed eEF1A (*146*).

Ribonucleoproteins. Alternative splicing results in multiple transcripts from a single gene, and can therefore generate additional diversity in an organism's protein complement. We have identified 269 genes for ribonucleoproteins. This represents over 2.5 times the number of ribonucleoprotein genes in the worm, two times that of the fly, and about the same as the 265 identified in the *Arabidopsis* genome. Whether the diversity of ribonucleoprotein genes in humans contributes to gene regulation at either the splicing or translational level is unknown.

Posttranslational modifications. In this set of processes, the most prominent expansion is the transglutaminases, calcium-dependent enzymes that catalyze the cross-linking of proteins in cellular processes such as hemostasis and apoptosis (*147*). The vitamin K–dependent gamma carboxylase gene product acts on the GLA domain (missing in the fly and worm) found in coagulation factors, osteocalcin, and matrix GLA protein (*148*). Tyrosylprotein sulfotransferases participate in the posttranslational modification of proteins involved in inflammation and hemostasis, including coagulation factors and chemokine receptors (*149*). Although there is no significant numerical increase in the counts for domains involved in nuclear protein modification, there are a number of domain arrangements in the predicted human proteins that are not found in the other currently sequenced genomes. These include the tandem association of two histone deacetylase domains in HD6 with a ubiquitin finger domain, a feature lacking in the fly genome. An additional example is the co-occurrence of important nuclear regulatory enzyme PARP (poly-ADP ribosyl transferase) domain fused to protein-interaction domains—BRCT and VWA in humans.

Concluding remarks. There are several possible explanations for the differences in phenotypic complexity observed in humans when compared to the fly and worm. Some of these relate to the prominent differences in the immune system, hemostasis, neuronal, vascular, and cytoskeletal complexity. The finding that the human genome contains fewer genes than previously predicted might be compensated for by combinatorial diversity generated at the levels of protein architecture, transcriptional and translational control, posttranslational modification of proteins, or posttranscriptional regulation. Extensive domain shuffling to increase or alter combinatorial diversity can provide an exponential

Table 19 (*Continued*)

Panther family/subfamily*	H	F	W	Y	A
MHC class I	22	0	0	0	0
MHC class II	20	0	0	0	0
Other immunoglobulin†	114	0	0	0	0
Toll receptor–related	10	6	0	0	0
Developmental and homeostatic regulators					
Signaling molecules†					
Calcitonin	3	0	0	0	0
Ephrin	8	2	4	0	0
FGF	24	1	1	0	0
Glucagon	4	0	0	0	0
Glycoprotein hormone beta chain	2	0	0	0	0
Insulin	1	0	0	0	0
Insulin-like hormone	3	0	0	0	0
Nerve growth factor	3	0	0	0	0
Neuregulin/heregulin	6	0	0	0	0
neuropeptide Y	4	0	0	0	0
PDGF	1	1	0	0	0
Relaxin	3	0	0	0	0
Stannocalcin	2	0	0	0	0
Thymopoeitin	2	0	1	0	0
Thyomosin beta	4	2	0	0	0
TGF-β	29	6	4	0	0
VEGF	4	0	0	0	0
Wnt	18	6	5	0	0
Receptors†					
Ephrin receptor	12	2	1	0	0
FGF receptor	4	4	0	0	0
Frizzled receptor	12	6	5	0	0
Parathyroid hormone receptor	2	0	0	0	0
VEGF receptor	5	0	0	0	0
BDNF/NT-3 nerve growth factor receptor	4	0	0	0	0
Kinases and phosphatases					
Dual-specificity protein phosphatase	29	8	10	4	11
S/T and dual-specificity protein kinase†	395	198	315	114	1102
S/T protein phosphatase	15	19	51	13	29
Y protein kinase†	106	47	100	5	16
Y protein phosphatase	56	22	95	5	6
Signal transduction					
ARF family	55	29	27	12	45
Cyclic nucleotide phosphodiesterase	25	8	6	1	0
G protein-coupled receptors†‡	616	146	284	0	1
G-protein alpha	27	10	22	2	5
G-protein beta	5	3	2	1	1
G-protein gamma	13	2	2	0	0
Ras superfamily	141	64	62	26	86
G-protein modulators†					
ARF GTPase-activating	20	8	9	5	15
Neurofibromin	7	2	0	2	0
Ras GTPase-activating	9	3	8	1	0
Tuberin	7	3	2	0	0
Vav proto-oncogene family	35	15	13	3	0

quence well into centromeric regions and allowed high-quality resolution of complex repeat regions. Likewise, in *Drosophila*, the BAC physical map was most useful in regions near the highly repetitive centromeres and telomeres. WGA has been found to deliver excellent-quality reconstructions of the unique regions of the genome. As the genome size, and more importantly the repetitive content, increases, the WGA approach delivers less of the repetitive sequence.

The cost and overall efficiency of clone-by-clone approaches makes them difficult to justify as a stand-alone strategy for future large-scale genome-sequencing projects. Specific applications of BAC-based or other clone mapping and sequencing strategies to resolve ambiguities in sequence assembly that cannot be efficiently resolved with computational approaches alone are clearly worth exploring. Hybrid approaches to whole-genome sequencing will only work if there is sufficient coverage in both the whole-genome shotgun phase and the BAC clone sequencing phase. Our experience with human genome assembly suggests that this will require at least 3× coverage of both whole-genome and BAC shotgun sequence data.

8.2 The low gene number in humans

We have sequenced and assembled ~95% of the euchromatic sequence of *H. sapiens* and used a new automated gene prediction method to produce a preliminary catalog of the human genes. This has provided a major surprise: We have found far fewer genes (26,000 to 38,000) than the earlier molecular predictions (50,000 to over 140,000). Whatever the reasons for this current disparity, only detailed annotation, comparative genomics (particularly using the *Mus musculus* genome), and careful molecular dissection of complex phenotypes will clarify this critical issue of the basic "parts list" of our genome. Certainly, the analysis is still incomplete and considerable refinement will occur in the years to come as the precise structure of each transcription unit is evaluated. A good place to start is to determine why the gene estimates derived from EST data are so discordant with our predictions. It is likely that the following contribute to an inflated gene number derived from ESTs: the variable lengths of 3′- and 5′-untranslated leaders and trailers; the little-understood vagaries of RNA processing that often leave intronic regions in an unspliced condition; the finding that nearly 40% of human genes are alternatively spliced (*153*); and finally, the unsolved technical problems in EST library construction where contamination from heterogeneous nuclear RNA and genomic DNA are not uncommon. Of course, it is possible that there are genes that remain unpredicted owing to the absence of EST or protein data to support them, although our use of mouse genome data for predicting genes should limit this number. As was true at the beginning of genome sequencing, ultimately it will be necessary to measure mRNA in specific cell types to demonstrate the presence of a gene.

J. B. S. Haldane speculated in 1937 that a population of organisms might have to pay a price for the number of genes it can possibly carry. He theorized that when the number of genes becomes too large, each zygote carries so many new deleterious mutations that the population simply cannot maintain itself. On the basis of this premise, and on the basis of available mutation rates and x-ray–induced mutations at specific loci, Muller, in 1967 (*154*), calculated that the mammalian genome would contain a maximum of not much more than 30,000 genes (*155*). An estimate of 30,000 gene loci for humans was also arrived at by Crow and Kimura (*156*). Muller's estimate for *D. melanogaster* was 10,000 genes, compared to 13,000 derived by annotation of the fly genome (*26*, *27*). These arguments for the theoretical maximum gene number were based on simplified ideas of genetic load—that all genes have a certain low rate of mutation to a deleterious state. However, it is clear that many mouse, fly, worm, and yeast knockout mutations lead to almost no discernible phenotypic perturbations.

The modest number of human genes means that we must look elsewhere for the mechanisms that generate the complexities inherent in human development and the sophisticated signaling systems that maintain homeostasis. There are a large number of ways in which the functions of individual genes and gene products are regulated. The degree of "openness" of chromatin structure and hence transcriptional activity is regulated by protein complexes that involve histone and DNA enzymatic modifications. We enumerate many of the proteins that are likely involved in nuclear regulation in Table 19. The location, timing, and quantity of transcription are intimately linked to nuclear signal transduction events as well as by the tissue-specific expression of many of these proteins. Equally important are regulatory DNA elements that include insulators, repeats, and endogenous viruses (*157*); methylation of CpG islands in imprinting (*158*); and promoter-enhancer and intronic regions that modulate transcription. The spliceosomal machinery consists of multisubunit proteins (Table 19) as well as structural and catalytic RNA elements (*159*) that regulate transcript structure through alternative start and termination sites and splicing. Hence, there is a need to study different classes of RNA molecules (*160*) such as small nucleolar RNAs, antisense riboregulator RNA, RNA involved in X-dosage compensation, and other structural RNAs to appreciate their precise role in regulating gene expression. The phenomenon of RNA editing in which coding changes occur directly at the level of mRNA is of clinical and biological relevance (*161*). Finally, examples of translational control include internal ribosomal entry sites that are found in proteins involved in cell cycle regulation and apoptosis (*162*). At the protein level, minor alterations in the nature of protein-protein interactions, protein modifications, and localization can have dramatic effects on cellular physiology (*163*). This dynamic system therefore has many ways to modulate activity, which suggests that definition of complex systems by analysis of single genes is unlikely to be entirely successful.

In situ studies have shown that the human genome is asymmetrically populated with G+C content, CpG islands, and genes (*68*). However, the genes are not distributed quite as unequally as had been predicted (Table 9) (*69*). The most G+C-rich fraction of the genome, H3 isochores, constitute more of the genome than previously thought (about 9%), and are the most gene-dense fraction, but contain only 25% of the genes, rather than the predicted ~40%. The low G+C L isochores make up 65% of the genome, and 48% of the genes. This inhomogeneity, the net result of millions of years of mammalian gene duplication, has been described as the "desertification" of the vertebrate genome (*71*). Why are there clustered regions of high and low gene density, and are these accidents of history or driven by selection and evolution? If these deserts are dispensable, it ought to be possible to find mammalian genomes that are far smaller in size than the human genome. Indeed, many species of bats have genome sizes that are much smaller than that of humans; for example, *Miniopterus*, a species of Italian bat, has a genome size that is only 50% that of humans (*164*). Similarly, *Muntiacus*, a species of Asian barking deer, has a genome size that is ~70% that of humans.

8.3 Human DNA sequence variation and its distribution across the genome

This is the first eukaryotic genome in which a nearly uniform ascertainment of polymorphism has been completed. Although we have identified and mapped more than 3 million SNPs, this by no means implies that the task of finding and cataloging SNPs is complete. These represent only a fraction of the SNPs present in the human population as a whole. Nevertheless, this first glimpse at genome-wide variation has revealed strong inhomogeneities in the distribution of SNPs across the genome. Polymorphism in DNA carries with it a snapshot of the past operation of population genetic forces, including mutation, migration, selection, and genetic drift. The availability of a dense array of SNPs will allow questions related to each of these factors to be addressed on a genome-wide basis. SNP studies can establish the range of haplo-

nome would open up new strategies for human biological research and would have a major impact on medicine, and through medicine and public health, on society. Effects on biomedical research are already being felt. This assembly of the human genome sequence is but a first, hesitant step on a long and exciting journey toward understanding the role of the genome in human biology. It has been possible only because of innovations in instrumentation and software that have allowed automation of almost every step of the process from DNA preparation to annotation. The next steps are clear: We must define the complexity that ensues when this relatively modest set of about 30,000 genes is expressed. The sequence provides the framework upon which all the genetics, biochemistry, physiology, and ultimately phenotype depend. It provides the boundaries for scientific inquiry. The sequence is only the first level of understanding of the genome. All genes and their control elements must be identified; their functions, in concert as well as in isolation, defined; their sequence variation worldwide described; and the relation between genome variation and specific phenotypic characteristics determined. Now we know what we have to explain.

Another paramount challenge awaits: public discussion of this information and its potential for improvement of personal health. Many diverse sources of data have shown that any two individuals are more than 99.9% identical in sequence, which means that all the glorious differences among individuals in our species that can be attributed to genes falls in a mere 0.1% of the sequence. There are two fallacies to be avoided: determinism, the idea that all characteristics of the person are "hard-wired" by the genome; and reductionism, the view that with complete knowledge of the human genome sequence, it is only a matter of time before our understanding of gene functions and interactions will provide a complete causal description of human variability. The real challenge of human biology, beyond the task of finding out how genes orchestrate the construction and maintenance of the miraculous mechanism of our bodies, will lie ahead as we seek to explain how our minds have come to organize thoughts sufficiently well to investigate our own existence.

References and Notes

1. R. L. Sinsheimer, *Genomics* **5**, 954 (1989); U.S. Department of Energy, Office of Health and Environmental Research, *Sequencing the Human Genome: Summary Report of the Santa Fe Workshop*, Santa Fe, NM, 3 to 4 March 1986 (Los Alamos National Laboratory, Los Alamos, NM, 1986).
2. R. Cook-Deegan, *The Gene Wars: Science, Politics, and the Human Genome* (Norton, New York, 1996).
3. F. Sanger *et al.*, *Nature* **265**, 687 (1977).
4. P. H. Seeburg *et al.*, *Trans. Assoc. Am. Physicians* **90**, 109 (1977).
5. E. C. Strauss, J. A. Kobori, G. Siu, L. E. Hood, *Anal. Biochem.* **154**, 353 (1986).
6. J. Gocayne *et al.*, *Proc. Natl. Acad. Sci. U.S.A.* **84**, 8296 (1987).
7. A. Martin-Gallardo *et al.*, *DNA Sequence* **3**, 237 (1992); W. R. McCombie *et al.*, *Nature Genet.* **1**, 348 (1992); M. A. Jensen *et al.*, *DNA Sequence* **1**, 233 (1991).
8. M. D. Adams *et al.*, *Science* **252**, 1651 (1991).
9. M. D. Adams *et al.*, *Nature* **355**, 632 (1992); M. D. Adams, A. R. Kerlavage, C. Fields, J. C. Venter, *Nature Genet.* **4**, 256 (1993); M. D. Adams, M. B. Soares, A. R. Kerlavage, C. Fields, J. C. Venter, *Nature Genet.* **4**, 373 (1993); M. H. Polymeropoulos *et al.*, *Nature Genet.* **4**, 381 (1993); M. Marra *et al.*, *Nature Genet.* **21**, 191 (1999).
10. M. D. Adams *et al.*, *Nature* **377**, 3 (1995); O. White *et al.*, *Nucleic Acids Res.* **21**, 3829 (1993).
11. F. Sanger, A. R. Coulson, G. F. Hong, D. F. Hill, G. B. Petersen, *J. Mol. Biol.* **162**, 729 (1982).
12. B. W. J. Mahy, J. J. Esposito, J. C. Venter, *Am. Soc. Microbiol. News* **57**, 577 (1991).
13. R. D. Fleischmann *et al.*, *Science* **269**, 496 (1995).
14. C. M. Fraser *et al.*, *Science* **270**, 397 (1995).
15. C. J. Bult *et al.*, *Science* **273**, 1058 (1996); J. F. Tomb *et al.*, *Nature* **388**, 539 (1997); H. P. Klenk *et al.*, *Nature* **390**, 364 (1997).
16. J. C. Venter, H. O. Smith, L. Hood, *Nature* **381**, 364 (1996).
17. H. Schmitt *et al.*, *Genomics* **33**, 9 (1996).
18. S. Zhao *et al.*, *Genomics* **63**, 321 (2000).
19. X. Lin *et al.*, *Nature* **402**, 761 (1999).
20. J. L. Weber, E. W. Myers, *Genome Res.* **7**, 401 (1997).
21. P. Green, *Genome Res.* **7**, 410 (1997).
22. E. Pennisi, *Science* **280**, 1185 (1998).
23. J. C. Venter *et al.*, *Science* **280**, 1540 (1998).
24. M. D. Adams *et al.*, *Nature* **368**, 474 (1994).
25. E. Marshall, E. Pennisi, *Science* **280**, 994 (1998).
26. M. D. Adams *et al.*, *Science* **287**, 2185 (2000).
27. G. M. Rubin *et al.*, *Science* **287**, 2204 (2000).
28. E. W. Myers *et al.*, *Science* **287**, 2196 (2000).
29. F. S. Collins *et al.*, *Science* **282**, 682 (1998).
30. International Human Genome Sequencing Consortium (2001), *Nature* **409**, 860 (2001).
31. Institutional review board: P. Calabresi (chairman), H. P. Freeman, C. McCarthy, A. L. Caplan, G. D. Rogell, J. Karp, M. K. Evans, B. Margus, C. L. Carter, R. A. Millman, S. Broder.
32. Eligibility criteria for participation in the study were as follows: prospective donors had to be 21 years of age or older, not pregnant, and capable of giving an informed consent. Donors were asked to self-define their ethnic backgrounds. Standard blood bank screens (screening for HIV, hepatitis viruses, and so forth) were performed on all samples at the clinical laboratory prior to DNA extraction in the Celera laboratory. All samples that tested positive for transmissible viruses were ineligible and were discarded. Karyotype analysis was performed on peripheral blood lymphocytes from all samples selected for sequencing; all were normal. A two-staged consent process for prospective donors was employed. The first stage of the consent process provided information about the genome project, procedures, and risks and benefits of participating. The second stage of the consent process involved answering follow-up questions and signing consent forms, and was conducted about 48 hours after the first.
33. DNA was isolated from blood (*173*) or sperm. For sperm, a washed pellet (100 μl) was lysed in a suspension (1 ml) containing 0.1 M NaCl, 10 mM tris-Cl–20 mM EDTA (pH 8), 1% SDS, 1 mg proteinase K, and 10 mM dithiothreitol for 1 hour at 37°C. The lysate was extracted with aqueous phenol and with phenol/chloroform. The DNA was ethanol precipitated and dissolved in 1 ml TE buffer. To make genomic libraries, DNA was randomly sheared, end-polished with consecutive BAL31 nuclease and T4 DNA polymerase treatments, and size-selected by electrophoresis on 1% low-melting-point agarose. After ligation to Bst XI adapters (Invitrogen, catalog no. N408-18), DNA was purified by three rounds of gel electrophoresis to remove excess adapters, and the fragments, now with 3′-CACA overhangs, were inserted into Bst XI-linearized plasmid vector with 3′-TGTG overhangs. Libraries with three different average sizes of inserts were constructed: 2, 10, and 50 kbp. The 2-kbp fragments were cloned in a high-copy pUC18 derivative. The 10- and 50-kbp fragments were cloned in a medium-copy pBR322 derivative. The 2- and 10-kbp libraries yielded uniform-sized large colonies on plating. However, the 50-kbp libraries produced many small colonies and inserts were unstable. To remedy this, the 50-kbp libraries were digested with Bgl II, which does not cleave the vector, but generally cleaved several times within the 50-kbp insert. A 1264-bp Bam HI kanamycin resistance cassette (purified from pUCK4; Amersham Pharmacia, catalog no. 27-4958-01) was added and ligation was carried out at 37°C in the continual presence of Bgl II. As Bgl II–Bgl II ligations occurred, they were continually cleaved, whereas Bam HI–Bgl II ligations were not cleaved. A high yield of internally deleted circular library molecules was obtained in which the residual insert ends were separated by the kanamycin cassette DNA. The internally deleted libraries, when plated on agar containing ampicillin (50 μg/ml), carbenicillin (50 μg/ml), and kanamycin (15 μg/ml), produced relatively uniform large colonies. The resulting clones could be prepared for sequencing using the same procedures as clones from the 10-kbp libraries.
34. Transformed cells were plated on agar diffusion plates prepared with a fresh top layer containing no antibiotic poured on top of a previously set bottom layer containing excess antibiotic, to achieve the correct final concentration. This method of plating permitted the cells to develop antibiotic resistance before being exposed to antibiotic without the potential clone bias that can be introduced through liquid outgrowth protocols. After colonies had grown, QBot (Genetix, UK) automated colony-picking robots were used to pick colonies meeting stringent size and shape criteria and to inoculate 384-well microtiter plates containing liquid growth medium. Liquid cultures were incubated overnight, with shaking, and were scored for growth before passing to template preparation. Template DNA was extracted from liquid bacterial culture using a procedure based upon the alkaline lysis miniprep method (*173*) adapted for high throughput processing in 384-well microtiter plates. Bacterial cells were lysed; cell debris was removed by centrifugation; and plasmid DNA was recovered by isopropanol precipitation and resuspended in 10 mM tris-HCl buffer. Reagent dispensing operations were accomplished using Titertek MAP 8 liquid dispensing systems. Plate-to-plate liquid transfers were performed using Tomtec Quadra 384 Model 320 pipetting robots. All plates were tracked throughout processing by unique plate barcodes. Mated sequencing reads from opposite ends of each clone insert were obtained by preparing two 384-well cycle sequencing reaction plates from each plate of plasmid template DNA using ABI-PRISM BigDye Terminator chemistry (Applied Biosystems) and standard M13 forward and reverse primers. Sequencing reactions were prepared using the Tomtec Quadra 384-320 pipetting robot. Parent-child plate relationships and, by extension, forward-reverse sequence mate pairs were established by automated plate barcode reading by the onboard barcode reader and were recorded by direct LIMS communication. Sequencing reaction products were purified by alcohol precipitation and were dried, sealed, and stored at 4°C in the dark until needed for sequencing, at which time the reaction products were resuspended in deionized formamide and sealed immediately to prevent degradation. All sequence data were generated using a single sequencing platform, the ABI PRISM 3700 DNA Analyzer. Sample sheets were created at load time using a Java-based application that facilitates barcode scanning of the sequencing plate barcode, retrieves sample information from the central LIMS, and reserves unique trace identifiers. The application permitted a single sample sheet file in the linking directory and deleted previously created sample sheet files immediately upon scanning of a

share at least one significant BLAST hit in common. This is an especially interesting property of the metric, because it allows the rapid recovery of protein families from the proteome for which no multiple alignment is possible, thus providing a computational basis for the extension of protein homology searches beyond those of current HMM- and profile-based search methods. Once the whole-proteome similarity matrix has been calculated, Lek first partitions the proteome into single-linkage clusters (27) on the basis of one or more shared BLAST hits between two sequences. Next, these single-linkage clusters are further partitioned into subclusters, each member of which shares a user-specified pairwise similarity with the other members of the cluster, as described above. For the purposes of this publication, we have focused on the analysis of single-linkage clusters and what we have termed "complete clusters," e.g., those subclusters for which every member has a similarity metric of 1 to every other member of the subcluster. We believe that the single-linkage and complete clusters are of special interest, in part, because they allow us to estimate and to compare sizes of core protein sets in a rigorous manner. The rationale for this is as follows: If one imagines for a moment a perfect clustering algorithm capable of perfectly partitioning one or more perfectly annotated protein sets into protein families, it is reasonable to assume that the number of clusters will always be greater than, or equal to, the number of single-linkage clusters, because single-linkage clustering is a maximally agglomerative clustering method. Thus, if there exists a single protein in the predicted protein set containing domains A and B, then it will be clustered by single linkage together with all single-domain proteins containing domains A or B. Likewise, for a predicted protein set containing a single multidomain protein, the number of real clusters must always be less than or equal to the number of complete clusters, because it is impossible to place a unique multidomain protein into a complete cluster. Thus, the single-linkage and complete clusters plus singletons should comprise a lower and upper bound of sizes of core protein sets, respectively, allowing us to compare the relative size and complexity of different organisms' predicted protein set.

90. T. F. Smith, M. S. Waterman, *J. Mol. Biol.* **147**, 195 (1981).
91. A. L. Delcher *et al.*, *Nucleic Acids Res.* **27**, 2369 (1999).
92. *Arabidopsis* Genome Initiative, *Nature* **408**, 796 (2000).

93. The probability that a contiguous set of proteins is the result of a segmental duplication can be estimated approximately as follows. Given that protein A and B occur on one chromosome, and that A′ and B′ (paralogs of A and B) also exist in the genome, the probability that B′ occurs immediately after A′ is $1/N$, where N is the number of proteins in the set (for this analysis, N = 26,588). Allowing for B′ to occur as any of the next J-1 proteins [leaving a gap between A′ and B′ increases the probability to $(J - 1)/N$; allowing B′A′ or A′B′ gives a probability of $2(J - 1)/N$]. Considering three genes ABC, the probability of observing A′B′C′ elsewhere in the genome, given that the paralogs exist, is $1/N^2$. Three proteins can occur across a spread of five positions in six ways; more generally, we compute the number of ways that K proteins can be spread across J positions by counting all possible arrangements of $K - 2$ proteins in the $J - 2$ positions between the first and last protein. Allowing for a spread to vary from K positions (no gaps) to J gives

$$L = \sum_{X=K-2}^{J-2} \binom{X}{K-2}$$

arrangements. Thus, the probability of chance occurrence is L/N^{K-1}. Allowing for both sets of genes (e.g., ABC and A′B′C′) to be spread across J positions increases this to L^2/N^{K-1}. The duplicated segment might be rearranged by the operations of reversal or translocation; allowing for M such rearrangements gives us a probability $P = L^2M/N^{K-1}$. For example, the probability of observing a duplicated set of three genes in two different locations, where the three genes occur across a spread of five positions in both locations, is $36/N^2$; the expected number of such matched sets in the predicted protein set is approximately $(N)36/N^2 = 36/N$, a value $\ll 1$. Therefore, any such duplications of three genes are unlikely to result from random rearrangements of the genome. If any of the genes occur in more than two copies, the probability that the apparent duplication has occurred by chance increases. The algorithm for selecting candidate duplications only generates matched protein sets with $P \ll 1$.

94. B. J. Trask *et al.*, *Hum. Mol. Genet.* **7**, 13 (1998); D. Sharon *et al.*, *Genomics* **61**, 24 (1999).
95. W. B. Barbazuk *et al.*, *Genome Res.* **10**, 1351 (2000); A. McLysaght, A. J. Enright, L. Skrabanek, K. H. Wolfe, *Yeast* **17**, 22 (2000); D. W. Burt *et al.*, *Nature* **402**, 411 (1999).
96. Reviewed in L. Skrabanek, K. H. Wolfe, *Curr. Opin. Genet. Dev.* **8**, 694 (1998).
97. P. Taillon-Miller, Z. Gu, Q. Li, L. Hillier, P. Y. Kwok, *Genome Res.* **8**, 748 (1998); P. Taillon-Miller, E. E. Piernot, P. Y. Kwok, *Genome Res.* **9**, 499 (1999).
98. D. Altshuler *et al.*, *Nature* **407**, 513 (2000).
99. G. T. Marth *et al.*, *Nature Genet.* **23**, 452 (1999).
100. W.-H. Li, *Molecular Evolution* (Sinauer, Sunderland, MA, 1997).
101. M. Cargill *et al.*, *Nature Genet.* **22**, 231 (1999).
102. M. K. Halushka *et al.*, *Nature Genet.* **22**, 239 (1999).
103. J. Zhang, T. L. Madden, *Genome Res.* **7**, 649 (1997).
104. M. Nei, *Molecular Evolutionary Genetics* (Columbia Univ. Press, New York, 1987).

105. From the observed coverage of the sequences at each site for each individual, we calculated the probability that a SNP would be detected at the site if it were present. For each level of coverage, there is a binomial sampling of the two homologs for each individual, and a heterozygous site could only be ascertained if both homologs are present, or if two alleles from different individuals are present. With coverage x from a given individual, both homologs are present in the assembly with probability $1 - (1/2)x^{-1}$. Even if both homologs are present, the probability that a SNP is detected is <1 because a fraction of sites failed the quality criteria. Integrating over coverage levels, the binomial sampling, and the quality distribution, we derived an expected number of sites in the genome that were ascertained for polymorphism for each individual. The nucleotide diversity was then the observed number of variable sites divided by the expected number of sites ascertained.

106. M. W. Nachman, V. L. Bauer, S. L. Crowell, C. F. Aquadro, *Genetics* **150**, 1133 (1998).
107. D. A. Nickerson *et al.*, *Nature Genet.* **19**, 233 (1998); D. A. Nickerson *et al.*, *Genomic Res.* **10**, 1532 (2000); L. Jorde *et al.*, *Am. J. Hum. Genet.* **66**, 979 (2000); D. G. Wang *et al.*, *Science* **280**, 1077 (1998).
108. M. Przeworski, R. R. Hudson, A. Di Rienzo, *Trends Genet.* **16**, 296 (2000).
109. S. Tavare, *Theor. Popul. Biol.* **26**, 119 (1984).
110. R. R. Hudson, in *Oxford Surveys in Evolutionary Biology*, D. J. Futuyma, J. D. Antonovics, Eds. (Oxford Univ. Press, Oxford, 1990), vol. 7, pp. 1–44.
111. A. G. Clark *et al.*, *Am. J. Hum. Genet.* **63**, 595 (1998).
112. M. Kimura, *The Neutral Theory of Molecular Evolution* (Cambridge Univ. Press, Cambridge, 1983).
113. H. Kaessmann, F. Heissig, A. von Haeseler, S. Paabo, *Nature Genet.* **22**, 78 (1999).
114. E. L. Sonnhammer, S. R. Eddy, R. Durbin, *Proteins* **28**, 405 (1997).
115. A. Bateman *et al.*, *Nucleic Acids Res.* **28**, 263 (2000).

116. Brief description of the methods used to build the Panther classification. First, the June 2000 release of the GenBank NR protein database (excluding sequences annotated as fragments or mutants) was partitioned into clusters using BLASTP. For the clustering, a seed sequence was randomly chosen, and the cluster was defined as all sequences matching the seed to statistical significance (E-value $< 10^{-5}$) and "globally" alignable (the length of the match region must be >70% and <130% of the length of the seed). If the cluster had more than five members, and at least one from a multicellular eukaryote, the cluster was extended. For the extension step, a hidden Markov Model (HMM) was trained for the cluster, using the SAM software package, version 2. The HMM was then scored against GenBank NR (excluding mutants but including fragments for this step), and all sequences scoring better than a specific (NLL-NULL) score were added to the cluster. The HMM was then retrained (with fixed model length) and all sequences in the cluster were aligned to the HMM to produce a multiple sequence alignment. This alignment was assessed by a number of quality measures. If the alignment failed the quality check, the initial cluster was rebuilt around the seed using a more restrictive E-value, followed by extension, alignment, and reassessment. This process was repeated until the alignment quality was good. The multiple alignment and "general" (i.e., describing the entire cluster, or "family") HMM (*176*) were then used as input into the BETE program (*177*). BETE calculates a phylogenetic tree for the sequences in the alignment. Functional information about the sequences in each cluster were parsed from SwissProt (*178*) and GenBank records. "Tree-attribute viewer" software was used by biologist curators to correlate the phylogenetic tree with protein function. Subfamilies were manually defined on the basis of shared function across subtrees, and were named accordingly. HMMs were then built for each subfamily, using information from both the subfamily and family (K. Sjölander, in preparation). Families were also manually named according to the functions contained within them. Finally, all of the families and subfamilies were classified into categories and subcategories based on their molecular functions. The categorization was done by manual review of the family and subfamily names, by examining SwissProt and GenBank records, and by review of the literature as well as resources on the World Wide Web. The current version (2.0) of the Panther molecular function schema has four levels: category, subcategory, family, and subfamily. Protein sequences for whole eukaryotic genomes (for the predicted human proteins and annotated proteins for fly, worm, yeast, and *Arabidopsis*) were scored against the Panther library of family and subfamily HMMs. If the score was significant (the NLL-NULL score cutoff depends on the protein family), the protein was assigned to the family or subfamily function with the most significant score.

117. C. P. Ponting, J. Schultz, F. Milpetz, P. Bork, *Nucleic Acids Res.* **27**, 229 (1999).
118. A. Goffeau *et al.*, *Science* **274**, 546, 563 (1996).
119. *C. elegans* Sequencing Consortium, *Science* **282**, 2012 (1998).
120. S. A. Chervitz *et al.*, *Science* **282**, 2022 (1998).
121. E. R. Kandel, J. H. Schwartz, T. Jessell, *Principles of Neural Science* (McGraw-Hill, New York, ed. 4, 2000).
122. D. A. Goodenough, J. A. Goliger, D. L. Paul, *Annu. Rev. Biochem.* **65**, 475 (1996).
123. D. G. Wilkinson, *Int. Rev. Cytol.* **196**, 177 (2000).
124. F. Nakamura, R. G. Kalb, S. M. Strittmatter, *J. Neurobiol.* **44**, 219 (2000).
125. P. J. Horner, F. H. Gage, *Nature* **407**, 963 (2000); P. Casaccia-Bonnefil, C. Gu, M. V. Chao, *Adv. Exp. Med. Biol.* **468**, 275 (1999).
126. S. Wang, B. A. Barres, *Neuron* **27**, 197 (2000).
127. M. Geppert, T. C. Sudhof, *Annu. Rev. Neurosci.* **21**, 75 (1998); J. T. Littleton, H. J. Bellen, *Trends Neurosci.* **18**, 177 (1995).
128. A. Maximov, T. C. Sudhof, I. Bezprozvanny, *J. Biol. Chem.* **274**, 24453 (1999).
129. B. Sampo *et al.*, *Proc. Natl. Acad. Sci. U.S.A.* **97**, 3666 (2000).
130. G. Lemke, *Glia* **7**, 263 (1993).
131. M. Bernfield *et al.*, *Annu. Rev. Biochem.* **68**, 729 (1999).
132. N. Perrimon, M. Bernfield, *Nature* **404**, 725 (2000).
133. U. Lindahl, M. Kusche-Gullberg, L. Kjellen, *J. Biol. Chem.* **273**, 24979 (1998).
134. J. L. Riechmann *et al.*, *Science* **290**, 2105 (2000).
135. T. L. Hurskainen, S. Hirohata, M. F. Seldin, S. S. Apte, *J. Biol. Chem.* **274**, 25555 (1999).

This Page is Inserted by IFW Indexing and Scanning Operations and is not part of the Official Record

BEST AVAILABLE IMAGES

Defective images within this document are accurate representations of the original documents submitted by the applicant.

Defects in the images include but are not limited to the items checked:

- ☐ BLACK BORDERS
- ☐ IMAGE CUT OFF AT TOP, BOTTOM OR SIDES
- ☐ FADED TEXT OR DRAWING
- ☐ BLURRED OR ILLEGIBLE TEXT OR DRAWING
- ☐ SKEWED/SLANTED IMAGES
- ☑ COLOR OR BLACK AND WHITE PHOTOGRAPHS
- ☐ GRAY SCALE DOCUMENTS
- ☐ LINES OR MARKS ON ORIGINAL DOCUMENT
- ☐ REFERENCE(S) OR EXHIBIT(S) SUBMITTED ARE POOR QUALITY
- ☐ OTHER: _____

IMAGES ARE BEST AVAILABLE COPY.
As rescanning these documents will not correct the image problems checked, please do not report these problems to the IFW Image Problem Mailbox.